INORGANIC CHEMISTRY

FRONTIERS

Accepted Manuscript

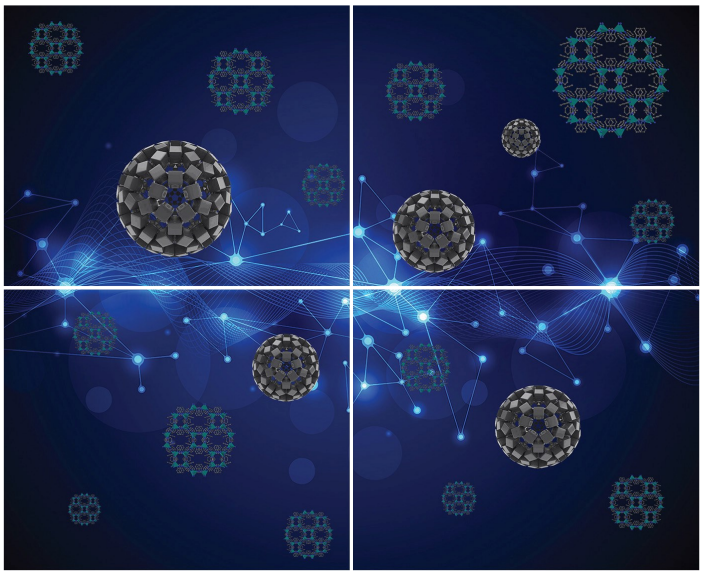

This article can be cited before page numbers have been issued, to do this please use: V. Gulino, A. Wolczyk, A. A. Golov, R. A. Eremin, M. Palumbo, C. Nervi, V. A. Blatov, D. M. Proserpio and M. Baricco, *Inorg. Chem. Front.*, 2020, DOI: 10.1039/D0QI00577K.

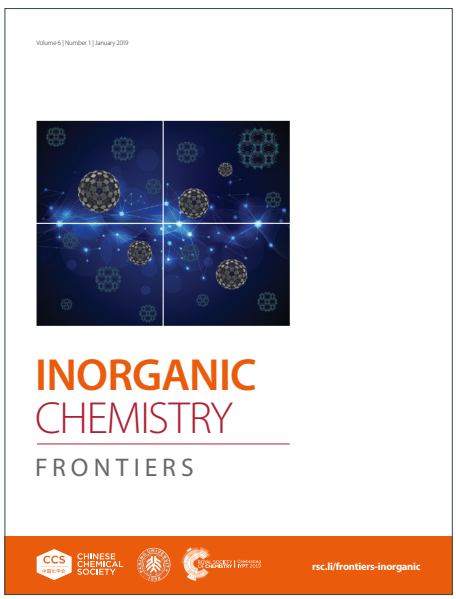

Combined DFT and Geometrical-Topological Analysis of Li-ion conductivity in Complex Hydrides

Valerio Gulino[1#], Anna Wolczyk[1#], Andrey A. Golov[2], Roman A. Eremin[2,3], Mauro Palumbo[1], Carlo Nervi[1], Vladislav A. Blatov[2,3*], Davide M. Proserpio[3,4] and Marcello Baricco[1]*

[1]Department of Chemistry and NIS, University of Turin, Via P. Giuria 9, I-10125 Torino, Italy

[2]Samara Center for Theoretical Materials Science, Samara University, Samara 443011, Russia

[3]Samara Center for Theoretical Materials Science, Samara State Technical University, Samara 443100, Russia

[4]Dipartimento di Chimica, Università degli studi di Milano, 20133, Milano, Italy

[#]co-first authors

[*]Corresponding authors:
Prof. Mauro PALUMBO
Department of Chemistry, University of Turin
Via Pietro Giuria, 9 I-10125 TORINO (Italy)
Tel. + 39 011 670 7097 Fax. + 39 011 670 7855
e-mail: mauro.palumbo@unito.it

Prof. Vladislav A. BLATOV
Samara Center for Theoretical Materials Science, Samara State Technical University
Samara 443100, Russia
Tel. +7 846 3356798 Fax: +7 846 2784400
e-mail: blatov@topospro.com

View Article Online
DOI: 10.1039/D0QI00577K

Abstract

On the basis of DFT calculations, the Li-ion migration was analyzed for $LiBH_4$, $LiNH_2$, Li_2NH, $Li_2BH_4NH_2$, $Li_4BH_4(NH_2)_3$ and $Li_5(BH_4)_3NH$ complex hydrides by means of the nudged elastic band method. In addition, a Voronoi-partition-based method, as implemented in the ToposPro program package, was adopted to determine cavities and channels in the complex hydrides and possible Li-ion migration pathways were computed. Experimental data for the Li-ion conductivity in the six compounds, measured by electrochemical impedance spectroscopy, have been taken from the literature and activation energies have been determined by a statistical analysis. A link between experimental and calculated activation energies has been evidenced, suggesting that topological analysis can provide good hints for the estimation of ion conductivity in complex hydrides.

Keywords: Li-ion conductivity, complex hydride, migration activation energy, nudged elastic band method, conductivity pathways, geometrical/topological analysis.

View Article Online
DOI: 10.1039/D0QI00577K

1. Introduction

Complex hydrides $M_x(XH_n)_y$ (where M is a metal cation, e.g. Li^+, and XH_n is a complex anion, e,g, $[BH_4]^-$, $[NH_2]^-$, $[NH]^{2-}$) cover a class of ionic compounds, which offers several energy-related applications, for example as potential hydrogen storage materials[1] to be used in future fuel cell technologies.[2] Recently, these compounds were suggested as electrolytes for all solid-state rechargeable batteries, owing not only to a high ionic conductivity coupled with a sufficient chemical and electrochemical stability, but also because of a strong compatibility with metallic Li.[3]

$LiBH_4$ shows an orthorhombic phase stable at room temperature (RT), with low Li-ion conductivity, as well as a hexagonal phase stable at temperatures higher than 110 °C, displaying superionic conductivity.[4] Different approaches have been applied in order to increase the Li-ion conductivity of these compounds. It can be achieved, for example, with stabilizing of the hexagonal phase by mixing it with halides[5,6] or creating a high conductive interface by mixing or nano-confining it with oxides.[7,8] New compounds can be also formed, as in the case of mixing $LiBH_4$ with lithium imide and amide.[9,10] In the system $LiBH_4$-$LiNH_2$, two complex hydrides are stable at RT, $Li_2(BH_4)(NH_2)$ and $Li_4(BH_4)(NH_2)_3$, and they exhibit lithium-ion conductivities higher than 10^{-4} S/cm at RT.[10–12] Considering the system $LiBH_4$-Li_2NH, Wolczyk et al.[9] reported the stability at RT of a novel compound, $Li_5(BH_4)_3NH$, that shows a Li-ion conductivity close to 10^{-6} S/cm at RT.

The Li-ion conductivity strictly depends on the energy barrier for diffusion, i.e. the minimum energy needed to complete a jump from one site to another in the crystal structure. Several approaches have recently been applied in the literature to obtain the value of this energy barrier and hence predict the ionic conductivity, such as the nudged elastic band (NEB) method,[13–15] *ab initio* molecular dynamics (AIMD) simulations,[16] or even the bond-valence (BV)[17] for high-throughput pre-screening analysis.

Topological methods have also been successfully applied to reveal new prospective Li- and Na-cation conductors with oxide anionic frameworks.[18–20] For this purpose, the combined geometrical/topological analysis, which uses the Voronoi partition of crystal space to convex polyhedra for searching for voids and channels available for mobile ions as well as the network analysis of the resulting migration map, was implemented in the ToposPro program package.[21] Since the topological approach is universal, it was successfully improved and extended to new classes of materials, including complex hydrides.[22,23]

Another route for an extension of semi-quantitative topological methods is to combine them with other simulation techniques, allowing the study of ionic transport properties at different levels of theory. We adopted the combination of experimental Solid State NMR with the computational *ab initio* modeling, namely density functional theory (DFT), to investigate the solid state properties of

View Article Online
DOI: 10.1039/D0QI00577K

metal hydrides and borohydrides.[12,24] Herein we aim to correlate ion conductivity with theoretical approaches, including the nudged elastic band (NEB) method, as implemented in various DFT packages, intended for studying energy characteristics of transition states by searching for minimum energy pathways.[14,15]

This paper aims to provide a comprehensive study of the Li-ion transport peculiarities in $LiBH_4$ $LiNH_2$, Li_2NH, $Li_2BH_4NH_2$, $Li_4BH_4(NH_2)_3$ and $Li_5(BH_4)_3NH$ complex hydrides, by a combined topological–DFT approach. In this study, we apply the Voronoi-based approach for searching for spatially available Li-ion migration pathways and for the calculation of their geometrical characteristics. The pathways are then explored by the NEB method to determine migration energies barriers and to build possible migration maps for the mobile cations. In addition, we use a topological approach to identify the topological type of the migration maps obtained by the NEB method. Results on activation energy for Li-ion conductivity obtained using computational methods have been compared with those obtained experimentally in the literature, providing additional insight on the mechanisms of ion mobility in complex hydrides.

2. Methodology

The crystal structures of $LiBH_4$ $LiNH_2$, Li_2NH, $Li_2BH_4NH_2$, $Li_4BH_4(NH_2)_3$ and $Li_5(BH_4)_3NH$ complex hydrides have been taken from the literature, as detailed in **Table S1** in Supporting Information.

To construct and explore migration maps for mobile Li^+ cations, we have used three methods of modeling, which are based on DFT methods, geometrical Voronoi partition and topological network approach.

2.1. DFT modeling

The method implemented in a step-by-step manner used within the current research was recently proposed and tested for solid state electrolytes.[25,26] The relaxation (cell shape/volume and atom positions) of the available crystal structures was performed using the projector-augmented wave approach with the Perdew-Burke-Ernzerhof (PBE)[27] exchange-correlation functional as implemented in Vienna Ab Initio Simulation Package (VASP).[28] The recommended pseudopotentials were used for each chemical element. The convergences of total energy value (the tolerance of 10^{-4} eV/atom), unit cell vector length and orientation (the tolerance of 10^{-3} Å with respect to the projections of the lattice vectors) were achieved with respect to plane-waves kinetic energy cutoff value (varying from 400 to 1000 eV with step of 200 eV) and density of the reciprocal space sampling within the Monkhorst–Pack (Γ-centered) scheme (the length parameter for automatic sampling procedure is varied from 10 to 30 Å with step of 5 Å). The energy cutoff of 600

View Article Online
DOI: 10.1039/D0QI00577K

eV and length parameter of 20 Å fitted the aforementioned convergency requirements for all systems studied.

At the next step, the optimized structures for the compounds under consideration were used for searching for migration pathways. In order to form the sets of independent Li–Li pathways, we have constructed the Voronoi partition for the Li sublattice ignoring all other atoms, as shown as an example in **Figure 1** for Li_2NH. In the Voronoi partition, each Li atom centers a convex Voronoi polyhedron, each internal point of which is closer to this Li than to other Li atoms of the sublattice. For each independent Li^+ (central) cation, we have accounted for all other $Li^+(i)$ cations, Voronoi polyhedra of which are adjacent to that of the Li^+(central), *i.e.* they have a common face, edge or vertex with the Li^+(central) Voronoi polyhedron. The longest Li^+(central)-$Li^+(i)$ distance defines the trusted radius, R_{trust}. Thus, the Voronoi partition was used here just to find the closest environment of a given Li^+ cation in the sublattice of mobile (Li^+) cations. Any jump of the Li^+(central) could be expected only to one of the neighboring Li^+ positions located inside the R_{trust} sphere that surrounds the Li^+(central). This approach does not fix the R_{trust} value, which can vary from one structure to another depending on the distribution of the mobile cations.

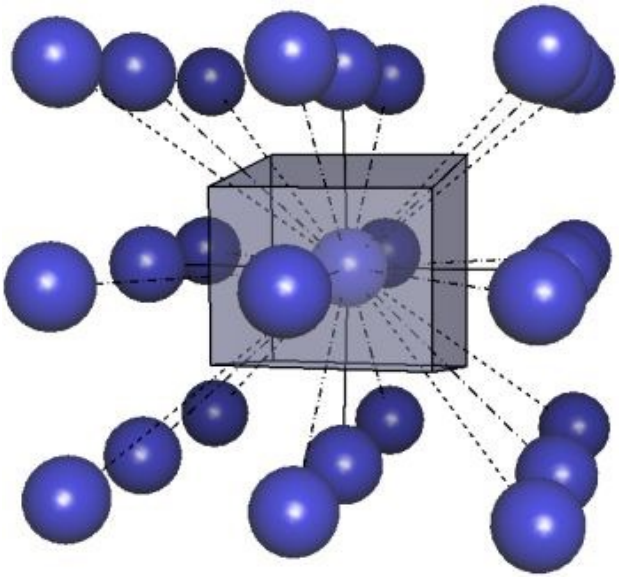

Figure 1. *The Voronoi polyhedron of a Li^+ cation in the Li sublattice of the Li_2NH crystal structure. The solid, dashed-dotted and dashed lines correspond to contacts between two Li^+ cations, which Voronoi polyhedra are adjacent by face, edge and vertex, respectively.*

After that, each symmetry-independent pathway was modeled as a transition of Li^+ from one vacant equilibrium position to another (which corresponds to an ion-vacancy exchange) and evaluated by means of the climbing image (CI) NEB method[14] as implemented in the CP2K code.[29] Three-dimensional periodic boundary conditions were applied for all modeled systems. All unit cells with

View Article Online
DOI: 10.1039/D0QI00577K

dimensions smaller than 8 Å were replaced by the corresponding supercells in order to exclude vacancy self-interaction. For the same reason, all the NEB runs were performed at the Γ-point of the reciprocal space.

For each pathway within the NEB modeling, eight replicas (images) were calculated using additional relaxation of the starting and ending replicas. The QuickStep[30] routine was used in the electron density calculations. The Goedecker-Tetter-Hutter pseudopotentials with the PBE exchange-correlation functional and the DZVP-MOLOPT-SR-GTH basis sets were chosen for all elements in the systems. The energy cutoff value of 800 Ry was applied. Three-dimensional periodic boundary conditions were applied with adding net charge of -1 electron charge value (due to Li^+ ion extraction). The tolerance on the maximum values of atom displacements and forces acting on atom of $2 \cdot 10^{-4}$ Å and $4.5 \cdot 10^{-4}$ Ha/bohr, respectively, and the maximum allowed RMS values of displacements and forces of 10^{-4} Å and $3 \cdot 10^{-4}$ Ha/bohr were chosen as the convergence control parameters for the NEB method.

For a particular pathway, the migration energy, E_m, was evaluated as the difference between the maximal value of the corresponding energy profile and the minimal energy value among all profiles obtained for the structure under consideration. Thus, possible energy differences of crystallographically inequivalent Li-ion vacancies, as well as possible favorable intermediate positions of the mobile ion, were taken into account. At the last stage, the pathways were sorted by their E_m values to obtain the energy limits for all possible periodicities of the migration map; each limit was determined as the maximum E_m value among all pathways, which formed the map.

From the migration energies, it is possible to derive the ionic conductivity σ in an isotropic medium as described in details by Goodenough et al.[31,32]. For ion-vacancy conduction, Ohm's law has the form:

$$j = \sigma E = N_V N q v, \quad (1)$$

where j is the current density, E is the applied electric field, N_V and N are the numbers of vacant sites and normal sites in the lattice, respectively, q is the ion charge and v is the moving ion velocity. The ionic conductivity can be then expressed as:

$$\sigma = N_V N q u, \quad (2)$$

where $u = v/E$, i.e. the charge-carrier mobility. Considering the Nernst-Einstein relationship for the mobility $u = qD/k_BT$ and the Arrhenius expression for the diffusion coefficient $D = D_0 e^{-E_m/k_BT}$, and introducing them into eq. (2) we obtain:

$$\sigma = \frac{\sigma_0'}{T} e^{-E_m/k_BT}, \quad (3)$$

View Article Online
DOI: 10.1039/D0QI00577K

where $\sigma'_0 = \left(\frac{Nq^2}{k}\right) N_V D_0 e^{-\Delta S_m/k_B T}$, ΔS_m is the migration entropy and k_B is the Boltzman constant.

Given the vacancy formation energy E_f and $N_V = Ae^{-E_f/k_B T}$ where A is a constant, by substituting into eq. (3) we finally obtain

$$\sigma = \frac{\sigma_0}{T} e^{-(E_m + E_f)/k_B T} = \frac{\sigma_0}{T} e^{-E_A/k_B T}, \quad (4)$$

where σ_0 is a pre-exponential factor and $E_A = E_m + E_f$ is the activation energy for ion-vacancy conduction. It can be seen that this activation energy depends both on the migration energy and the vacancy formation energy.

The latter was calculated using DFT according to the formalism detailed in by Van de Walle et al.[33] for a defect or impurity *X* in charge state *q*:

$$E_f[X^q] = E_{tot}[X^q] - E_{tot}[perfect] - \sum_i n_i \mu_i + qE_F, \quad (5)$$

where $E_{tot}[X^q]$ is the total energy obtained from a supercell DFT calculation with one impurity or defect *X*, $E_{tot}[perfect]$ is the total energy for the equivalent supercell without defects, n_i is the number of atoms of type *I* (host atoms or impurity) that have been added to ($n_i > 0$) or removed from ($n_i < 0$) the supercell when the defect or impurity is created and μ_i are the corresponding chemical potentials of these species. These chemical potentials represent the energy of the reservoir with which atoms are being exchange and can be determined from the experimental conditions in which the defect creation occurs. Finally, E_F is the Fermi level, also referred to as the electronic chemical potential referenced to the valence band maximum in the bulk. Note that E_F is not a free parameter, i.e. cannot be freely varied, but it is ultimately determined by the condition of charge neutrality. For a neutral defect (q=0), it does not affect the vacancy formation energy in eq. (5).

This formalism can be applied to neutral and charged defects, vacancies and interstitial atoms and was here used to obtain the formation energies for the relevant defects, as described in the following. For these supercell calculations, the VASP code was used with the same settings as described above for the relaxation of the crystal structures, except for the k-point meshes for the reciprocal space sampling, which were appropriately reduced maintaining the same target accuracy. After introducing the defect, each supercell was relaxed with respect to the ionic positions, while keeping the cell parameters of the perfect bulk. For charged defects calculations, a compensating uniform background (jellium) is imposed to restore charge neutrality in the system.[34]

2.2. Geometrical modeling

In the DFT approach, the migration pathways were selected among all geometrically possible jumps of Li^+ cations after relaxation of the structure in accordance with the energy criteria. To support the results obtained we applied an independent approach, which is based on the analysis of the Voronoi

net, which is formed by vertices and edges of the Voronoi polyhedra of all (framework) atoms except mobile cations as shown in **Figure 2a** and **Figure 2b** for Li_2NH.[18] By definition, the vertices and edges of Voronoi polyhedra represent the points of the crystal space, which are most distant from the framework atoms and, hence, mimic possible migration paths for mobile ions. This approach is somewhat opposite to the Voronoi method of searching for possible Li^+ migration paths in the DFT modeling described above. Here Li^+ cations should be excluded from consideration to leave possible migration channels free for the geometrical analysis, while in the DFT analysis only the Li^+ sublattice should be considered with the Voronoi method just to find the starting and ending points for the NEB trajectories.

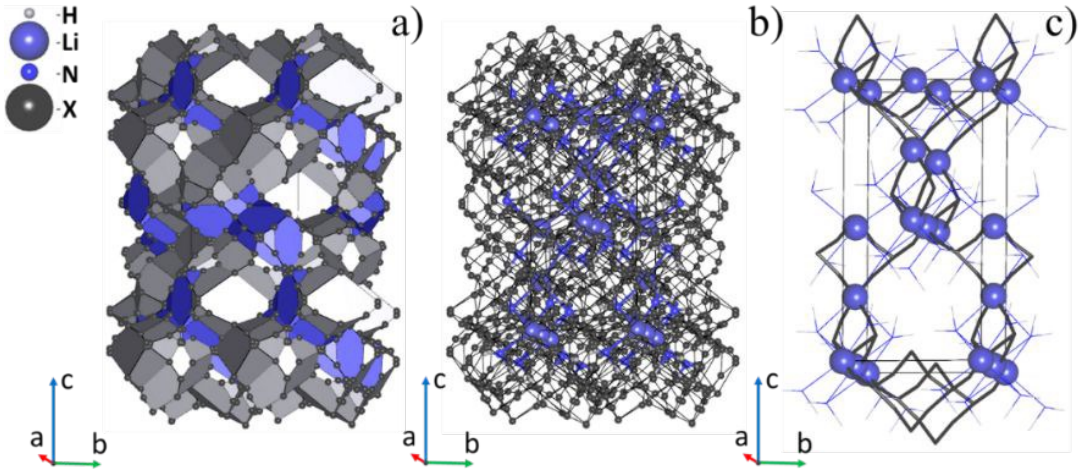

Figure 2. *a) The Voronoi polyhedra constructed for H and N atoms in the Li_2NH structure, b) the Voronoi net formed by vertices and edges of the atomic Voronoi polyhedra, c) the Voronoi subnet that corresponds to the widest three-periodic channels system. The X points correspond to the vertices of the polyhedra.*

At the second step, the radii of cavities and channels were evaluated. This step included the calculation of distances from nodes and edges of the Voronoi net to the closest atom, accounting for its radius; the distances reduced by the atom radius corresponded to cavities and channels radii, respectively. Since the ionic radii are not well estimated for hydrides, we used the Slater radii,[35] as previously applied successfully for the analysis of ion migration.[18,19] In order to take into account lability and polarizability of structural groups, an empirical correction was applied to the radii of channels (see section 3.2). The correction obtained was then used for all complex hydrides under consideration.

View Article Online
DOI: 10.1039/D0QI00577K

The third step comprised the search for a periodic system of channels that are available for migration of mobile ions. For this purpose, all the channels and cavities of the radii, which were smaller than the radius of the mobile ion, were removed.

Further, the non-periodic (finite) systems of channels and cavities were removed. The remaining infinite channel systems were assumed to be available for migration. Additionally, the Voronoi subnets that correspond to the widest periodic channels system, available for ion migration, were found. For this purpose, the nodes and edges of the net were sorted in ascending of their radii. Then the nodes or edges of the net with a minimal value of radius (*i.e.* the narrowest part of channel) were removed. This procedure was repeated until the periodicity of the subnet decreased. The subnet of channels obtained at the previous step of the procedure was assumed the widest for the given periodicity, as shown in **Figure 2c** for Li_2NH.

2.3. Topological analysis

The topological analysis of the migration maps was carried out with the ToposPro package.[21] For this purpose, one-, two- and three-periodic nets corresponding to the lowest energy migration maps were constructed based on the results of the NEB and geometrical analyses. To identify topological type of the migration map, the corresponding net was simplified by removing one- and two-coordinated nodes and a set of topological descriptors were calculated for the simplified nets.[36] The topological type of the migration maps was identified by comparing the calculated set of descriptors with those from the ToposPro topological type collection (TTD). The nomenclatures of the topological types as the RCSR bold three-letter symbols (e.g. **sql** or **hcb**), Fischer and Koch's symbols of low-periodic sphere packings (e.g. $6^3(0,2)$), or ToposPro TTD symbols (e.g. *sqc*2-7-*Cmmm*) were described in detail elsewhere.[37–39] This approach provides the information on the channels, which is essentially independent of their geometrical distortion and space group symmetry.

Thus, the three methods described above supplement each other as the geometrical approach enables one to estimate the possible positions for the NEB modeling, and the resulting NEB migration map is analyzed by the topological methods.

3. Results and Discussion

3.1. Migration energy limits

After relaxation, the relative deviations of cell dimensions less than 3% with respect to the experimentally available ones were obtained and no significant crystal structure changes were

observed for the compounds modeled. The resulting unit cell multiplicities, total numbers of the calculated independent pathways, distances of the longest transition, R_{trust} (in brackets) are listed in **Table 1**.

	Compound		$LiBH_4$	$LiNH_2$	Li_2NH	$Li_2NH_2BH_4$	$Li_4(NH_2)_3BH_4$	$Li_5(BH_4)_3NH$
CI-NEB	Supercell		2x2x2	2x2x1	2x2x2	1x1x1	1x1x1	1x1x2
	Total number of pathways (R_{trust}, Å)		5 (5.43)	8 (5.148)	9 (4.35)	46 (7.932)	15 (5.712)	26 (5.870)
	Migration energy limit, eV (number of pathways in a map)	1D	-	-	-	-	-	0.34 (3)
		2D	0.24 (1)	-	0.31 (2)	-	-	0.48 (6)
		3D	0.30 (2)	0.46 (2)	0.32 (3)	0.53 (5)	0.30 (2)	0.56 (10)
	The radius (Å) of the narrowest part of the widest one-, two-, or three-periodic channel systems.	1D	1.214	-	1.326	1.245	-	1.387
		2D	1.168	-	-	-	-	-
		3D	1.153	1.305	1.224	1.191	1.280	1.362

"iD" symbols correspond to a certain periodicity of migration map; "-" denotes that the map with a certain periodicity is not observed.

Table 1. *The Li-ion mobility parameters obtained from DFT and ToposPro calculations.*

The calculated total energy profiles of the minimal number of independent pathways, which are required to form a three-periodic migration map, are shown in **Figure 3**. The corresponding migration energy limits for certain periodicities of migration maps and numbers of the pathways involved in these maps (in brackets) are given in **Table 1**.

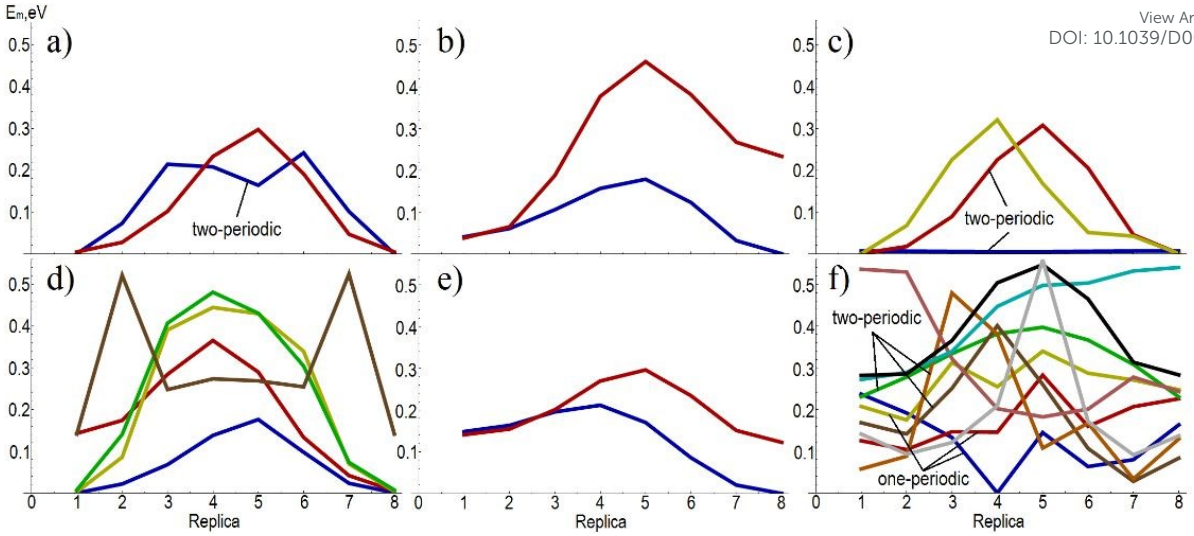

Figure 3. *The CI-NEB total energy profiles for the independent pathways, which are required to form the three-periodic migration maps in the a) $LiBH_4$, b) $LiNH_2$, c) Li_2NH, d) $Li_2BH_4NH_2$, e) $Li_4BH_4(NH_2)_3$, and f) $Li_5(BH_4)_3NH$ structures. The presented profiles are obtained after subtraction of the minimum energy among the three-periodic map pathways in the given structure.*

3.2. Geometrical analysis

According to the results of the NEB calculation, all considered complex hydrides possess three-periodic ionic conductivity, hence lithium cations move in a three-periodic channel system. The largest difference between Li radius (1.450 Å) and the radius of the narrowest channel in the widest three-periodic channel systems is 0.297 Å (**Table 1**). Thus, a value of 0.3 Å was chosen as the empirical correction of the channels radii to fit the results of the NEB calculations. This correction allows one to account for ion polarizability and relaxation of the atomic environment along the pathway during diffusion.

3.3 Topological analysis

3.3.1. $LiBH_4$

The $LiBH_4$ structure has two inequivalent lowest energy migration pathways (**Figure S1**). The pathways with the migration energy of 0.24 eV (**Figure S1a**) form a two-periodic (100) migration map with the **sql** topology (**Figure S2**). The pathways with the migration energy of 0.30 eV form zigzag [010] chains (**Figure S1b**). The chains connect the **sql** migration layers into a three-periodic migration map of the **acs** topology (**Figure S3**).

3.3.2. $LiNH_2$

The $LiNH_2$ structure has two inequivalent Li^+ migration pathways (**Figure S4**), which form a three-periodic migration map of the **tfa** topology (**Figure S5**). The migration map consists of (001) layers with the **sql** topology and the layers are connected by bridging pathways. The bridging pathways

have the migration energy of 0.18 eV (**Figure S4a**), whereas the migration layers are formed by the pathways with a higher migration energy of 0.46 eV (**Figure S5b**).

3.3.3. Li_2NH

In the crystal structure of Li_2NH, there are three inequivalent Li^+ migration pathways (**Figure S6**), which form the lowest energy two- (**Figure S7**) and three- periodic (**Figure S8**) migration maps. The set of the pathways with the lowest migration energy of 0.007 eV gives rise to a non-periodic migration map, which does not provide conductivity (**Figure S6a**). However, together with chain pathways [010] with the migration energy of 0.31 eV (**Figure S6b**) they form two-periodic (001) layers (**Figure S7**) with the **hcb** topology. Addition of the pathway with the migration energy of 0.32 eV (**Figure S6c**) leads to a three-periodic migration map of the *sqc*2-7-*Cmmm* topology (**Figure S8**). It is worth noting that the latest accounted pathway individually forms two independent two-periodic (010) layers of the **sql** topology.

3.3.4. $Li_2BH_4NH_2$

The $Li_2BH_4NH_2$ structure has five inequivalent Li^+ migration pathways (**Figure S9**). Separately, each pathway does form no periodic pattern. Nevertheless, taken together they form a three-periodic migration map. The topology of the map is described by a 6-coordinated uninodal net with the $(3^{10}.8^4.9)$ point symbol (**Figure S10**).

3.3.5. $Li_4BH_4(NH_2)_3$

The $Li_4BH_4(NH_2)_3$ crystal structure has two inequivalent Li^+ migration pathways (**Figure S11**). The pathways with migration energy of 0.30 eV (**Figure S11b**) form a three-periodic migration system of the **srs** topology, while the lowest energy pathways of 0.21 eV (**Figure S11a**) are terminal (**Figure S14**) and do not influence the conductivity.

3.3.6. $Li_5(BH_4)_3NH$

The $Li_5(BH_4)_3NH$ crystal structure has a quite complicated migration system, containing ten inequivalent pathways (**Figure S13**). Three of them (**Figure S13a-c**) form an one-periodic [100] migration map of the $6^3(0,2)$ topology (**Figure S14**). Six inequivalent migration pathways (**Figure S13a-f**) form a two-periodic (010) migration map (**Figure S15**), which is characterized by a 5,6-coordinated binodal net with the $(3^2.4^4.5^4)(3^4.4^6.5.6^4)$ point symbol. The three-periodic migration map (**Figure S16**) of the topology, which is described by a three-periodic 4, 7, 8-coordinated three-nodal net with the $(3^2.4^4)(3^6.4^5.5^4.6^5.7)_2(3^8.4^{14}.5^6)_2$ point symbol, is formed by all ten inequivalent migration pathways.

View Article Online
DOI: 10.1039/D0QI00577K

3.4 Experimental data of Li-ion conductivity

A survey of experimental data on Li-ion conductivity reported in the literature was performed for each compound studied in this work. As experimental results of Li-ion conductivity and activation energy show significant scatter, a statistical analysis was carried out before comparison with theoretical findings, as described in Supporting Information. For all compounds except $LiBH_4$, only a few Electrochemical Impedance Spectroscopy (EIS) measurements are reported in literature. Results of the statistical analysis are reported in **Table 2**.

As shown in **Figure S17,** several EIS measurements of the Li-ion conductivity of orthorhombic $LiBH_4$ are reported in the literature, showing a significant scatter. As an example, data span from 5×10^{-8} S/cm to 7×10^{-7} S/cm at 70 °C, within more than an order of magnitude range. Unfortunately, details about experimental conditions regarding these measurements are often not reported in the original papers, hence results can arise from different experimental conditions and sample preparation methods.

A further experimental parameter to be considered is the application of mechanical milling. In fact, ball-milled samples show usually higher ion conductivity with respect to non-milled samples (**Figure S17**).[40,41] The main explanation of the increased Li-ion conductivity is that the mechanochemical treatment increases the defect concentration of the orthorhombic $LiBH_4$.[7,41] The effect of ball milling on Li-ion conductivity in maintained if the sample is heated up to a temperature lower than the phase transition, as reported by Sveinbjörnsson et al.[41] On the contrary, the higher ionic conductivity due to the mechanical milling effect is reduced after the phase transition, as reported by Matsuo et al.[40] and Gulino et al.[7] In fact, once the milled samples undergo the phase transition, defects are recovered and the Li-ion conductivity decrease.[7] Therefore, the data of the ball-milled samples have been excluded in the calculation of the average values reported in **Table 2**.

The temperature dependence of ionic conductivity σ is related to the activation energy (E_A) according to eq. (4), as described in the Methodology Section. From EIS measurements reported in the literature, the activation energy (E_A) and the logarithm of the pre-exponential factor ($\ln \sigma_0$) were obtained by a linear fit of an Arrhenius plot for Eq. (1), by plotting the $\ln(\sigma T)$ as a function of 1000/T. A confidence interval was obtained from the linear fitting for both values of E_A and $\ln \sigma_0$. This interval was calculated using a confidence level of 99.99 %. For each EIS measurements, the confidence level was chosen in order to include all the experimental points inside the interval, *e.g.* as shown in **Figure S18**.

Regarding $LiBH_4$, the activation energies obtained from single set of data are reported in **Table S2**, while the values of the logarithm of the pre-exponential factor are shown in **Table S3**. Using the

confidence interval for each EIS measurement, it was also possible to calculate a maximum and minimum value of ln(σT), by using the maximum and minimum values, given by the confidence interval, of both E_A and ln σ_0. From these values, it was possible to calculate σ at 30 °C and a confidence interval associated to it, as reported in **Table S4**. For $LiNH_2$, Li_2NH, $Li_2(NH_2)(BH_4)$ and $Li_4(NH_2)_3(BH_4)$ complex hydrides, both E_A and ln σ_0 values obtained from EIS measurements reported in the literature are shown in **Table S5**, whereas σ at 30 °C is reported in **Table S6**.

From the statistical analysis, it was possible to obtain average values, for each compound, of the Li-ion conductivity at 30 °C, the activation energy (E_A) and the logarithm of pre-exponential factor (ln σ_0) (**Table 2**). For the $LiBH_4$ compound, the data obtained from literature EIS measurements of ball-milled $LiBH_4$, have been excluded in the calculation of the average value. Note that for $Li_5(BH_4)_3NH$ only one measurement has been reported in the literature. Therefore, the value reported in **Table 2**, is not an average value, but corresponds to the value associated to the single measurement reported by Wolczyk et al.[9]. In some cases, the confidence interval for E_A is > 0.05, which is relatively high compared to the corresponding values for E_A (i.e. up to 10%) and confirms the existence of a large scatter in experimental results from different sources.

Compound	Li-ion conductivity at 30 °C (S/cm)		E_A (eV)		ln σ_0	
$LiBH_4$	9.5×10^{-9}	$\pm 2.07\times10^{-9}$	0.75	± 0.07	16	± 2
$LiNH_2$	5.36×10^{-11}	$\pm 4.11\times10^{-11}$	0.98	± 0.06	19	± 2
Li_2NH	3.66×10^{-4}	$\pm 8.92\times10^{-5}$	0.60	± 0.04	21	± 2
$Li_2NH_2BH_4$	1.01×10^{-4}	$\pm 1.63\times10^{-5}$	0.69	± 0.06	23	± 2
$Li_4(NH_2)_3BH_4$	1.54×10^{-4}	$\pm 4.09\times10^{-5}$	0.37	± 0.02	10.1	± 0.6
$Li_5(BH_4)_3NH$	1.29×10^{-7}	$\pm 8.33\times10^{-8}$	0.73	± 0.03	18	± 2

Table 2. *The average values of Li-ionic conductivity at 30 °C, activation energy (E_A) and ln σ_0 obtained by the statistical analysis performed for the different investigated complex hydrides.*

3.5 Comparison between computed and experimental data

Possible relationships between values obtained experimentally and reported in the literature, (e.g. ionic conductivity at 30 °C and activation energy) and values calculated from the ToposPro output

(e.g. channels radius and migration energy) are investigated, in order to obtain some insight into the link occurring between Li^+ ion conductivity and the topological properties of the corresponding crystal structures.

Using the data reported in **Table 2**, a possible relationship between channel radii (as obtained from different periodicity) and values of Li-ion conductivity at 30 °C for the series of the compounds investigated ($LiBH_4$, $LiNH_2$, Li_2NH, $Li_2BH_4NH_2$, $Li_4BH_4(NH_2)_3$ and $Li_5(BH_4)_3NH$) is shown in **Figure 4**.

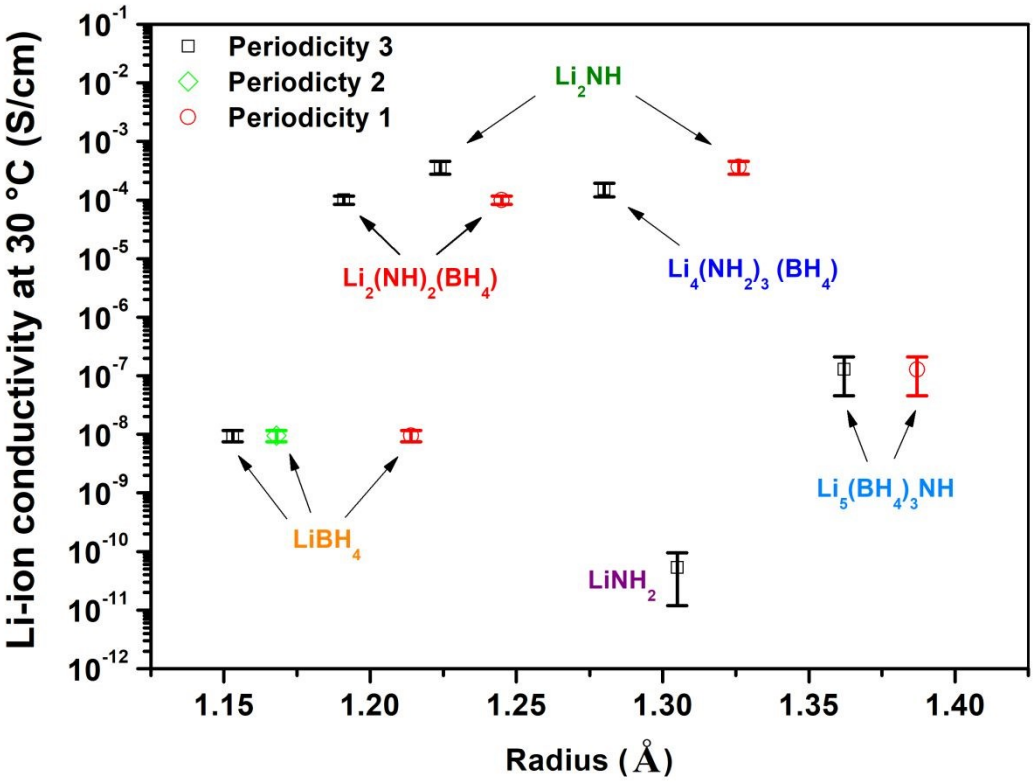

Figure 4. *Li-ion conductivity at 30 °C as a function of the radius of the narrowest part of the widest one-, two-or three-periodic channels in structures of $LiBH_4$, $LiNH_2$, Li_2NH, $Li_2BH_4NH_2$, $Li_4BH_4(NH_2)_3$ and $Li_5(BH_4)_3NH$.*

It is not possible to extract a clear trend from this figure, suggesting that the absolute value of Li-ion conductivity close to room temperature (i.e. at 30 °C) cannot be easily explained in terms of channel sizes in the structure. In fact, a significant contribution of the anionic species to the Li-ion conduction have been suggested for complex hydrides[42] on the basis of the so-called "paddle-wheel" mechanism.[43] In fact, it should be emphasized that, although the crystal structures of $Li_2BH_4NH_2$ (*trigonal*) and $Li_4BH_4(NH_2)_3$ (*cubic*) are rather different from those of the $LiBH_4$ (*orthorhombic*) and $LiNH_2$ (*tetragonal*), the combination of anions containing hydrogen, i.e. $(BH_4)^-$

and $(NH_2)^-$, could provide new occupation sites for Li^+ ions, which can account for their high mobility.[11] $LiNH_2$ is characterized by a low ion mobility, because the $[NH_2]^-$ groups block the channels for Li^+ diffusion.[44]

A comparison between calculated values for the migration energy and the experimental activation energy for Li-ion conductivity is reported in **Figure 5.** As already described, the activation energy was determined by statistical analysis of literature results, whereas the migration energy limit was calculated from DFT, considering both 3D and 2D periodicity, as reported in **Table 1**. It can be noticed that, as for the quantities shown in **Figure 4,** also in this case there is no clear correlation between the calculated and experimental values, the latter being consistently and significantly higher than the calculated migration energies. The error bar associated to experimental values is large, as already pointed out, but not enough to account for the difference with computed values.

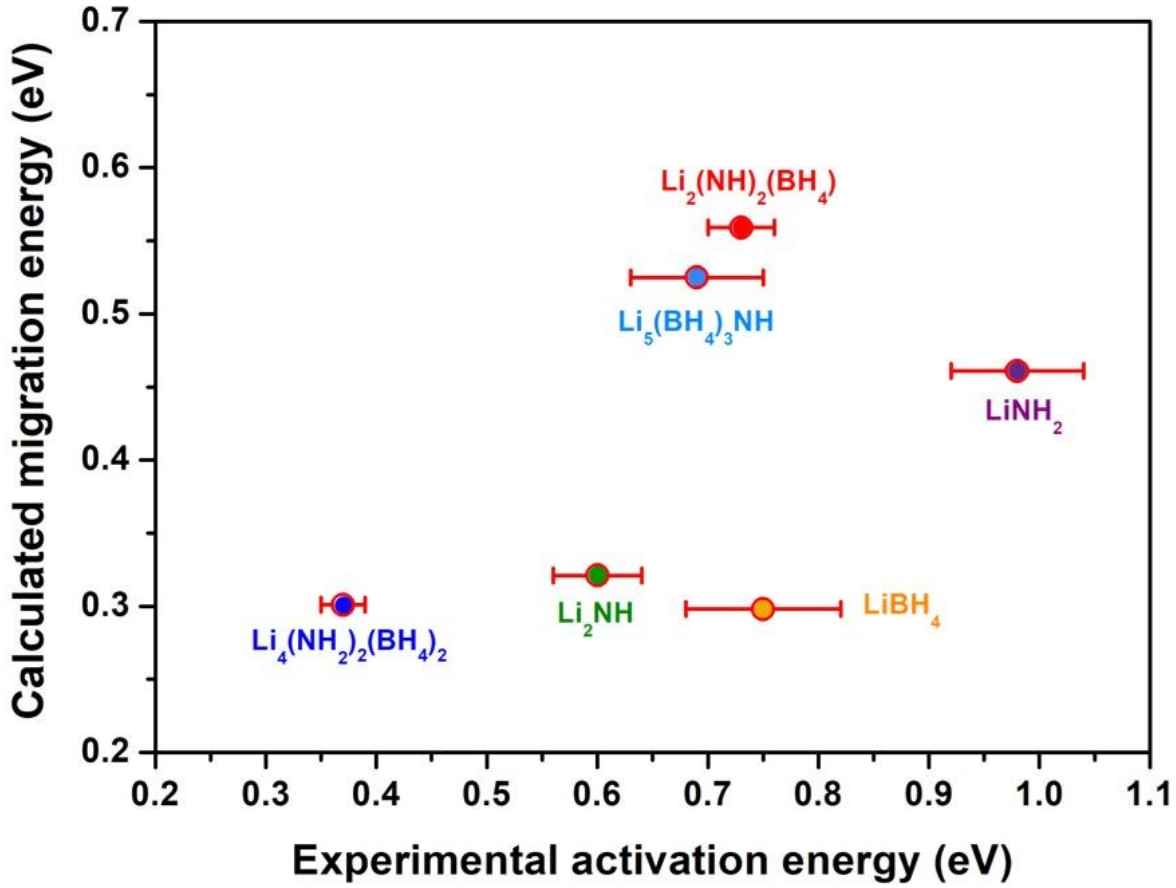

Figure 5. *Relationship between the migration energy limit calculated from DFT for $LiBH_4$, $LiNH_2$, Li_2NH, $Li_2BH_4NH_2$, $Li_4BH_4(NH_2)_3$, and $Li_5(BH_4)_3NH$and activation energy determined by a statistical analysis of literature data.*

View Article Online
DOI: 10.1039/D0QI00577K

The obtained values of the E_m limits of migration maps formation (**Table 1**) are expected to underestimate the experimentally available E_a values, since the proposed approach does not include the energy contribution to the defect formation.

To further investigate this point, we have first analyzed theoretical results for the defect formation previously reported in the literature for the systems studied in this work **(Table 3**). Note that no data have been found in the literature for $Li_2BH_4NH_2$, $Li_4BH_4(NH_2)_3$, and $Li_5(BH_4)_3NH$ compounds, so the analysis has been limited to $LiNH_2$, $LiBH_4$ and Li_2NH complex hydrides.

Compound	Ref	E_f Li_i^+ or V_{Li}^- (eV)	E_f Frenkel pair (eV)	Min. distance (Frenkel pair)	E_m (eV)	E_A (eV)
$LiNH_2$	([45])	0.51	0.65	0.85 Å	0.2-0.3	0.71-0.81
	([46])	0.57	0.72	/	0.46	1.03
	([47])	0.52	0.79	/	0.44	0.96
	([48])	0.49#	0.97	/	0.22-0.42	0.71-0.91
	([44])	/	/	/	0.38	/
	Present work	0.45	0.90	∞	0.46	0.91
$LiBH_4$	([49])	0.5	0.95	4.2 Å	0.3	0.8
	([50])	0.6#	1.2	∞	0.1-0.3	0.7-0.9
			0.88	4 Å		
	Present work	0.5	1.0	∞	0.30	0.80
Li_2NH	([44])	0.24#	0.48	/	0.17-0.47	0.41-0.71
	Present work	0.37	0.74	∞	0.32	0.69

#*Calculated dividing by 2 the E_f Frenkel pair*

Table 3. *Defect formation and migration energies reported in the literature and calculated in this work for the considered systems. E_f is the formation energy for a single vacancy (V_{Li}^-), or equivalently for a single*

View Article Online
DOI: 10.1039/D0QI00577K

interstitial Li_i^+ and for a Frenkel couple (see the text for details). E_m is the migration energy of Li ions calculated in this work. Where available, the minimum distance between the vacancy and the interstitial atom in a Frenkel couple is also reported. E_A is the activation energy obtained using Eq. (4). Note that the formation energy of Frenkel pair with finite distance (or not reported in the original paper) do not equal two times the formation energy of a single defect.

Calculated migration energies from the literature are also shown in Table 3 for comparison with our results and we can note that there is a satisfactory agreement between them. For example, Cho et al.[50] reported similar values for $LiBH_4$, in the range 0.1-0.3 eV, depending on the diffusion mechanism and paths. The value of 0.3 eV reported by Hoang et al.[49] is matching our result. For $LiNH_2$, several results are available from different authors within the range 0.20-0.46 eV, with our calculated value falling in the range, but close to the highest value.

The relevant possible defects for Li ion conductions are neutral lithium vacancies (V_{Li}), neutral lithium interstitials (Li_i) and the corresponding plus/minus one charged defects (V_{Li}^-, V_{Li}^+, Li_i^-, Li_i^+). In all studies reported in **Table 3** and in the present work, the combination of V_{Li}^- and Li_i^+, also known as a Frenkel pair, has been found to be the most stable. We then assume this as a common mechanism for all examined compounds.

Regarding the defect formation energies, it is worth noting that different approaches can be used to obtain such energies from the DFT calculations. For example, most of the values in **Table 3** have been calculated following an approach proposed by Van de Walle et al.[33], which has been described in the Methodology Section and used in our own calculations. This method has been used in Refs.[44–49]. According to this approach, the formation energy of a single charged isolated defect can be plotted as a function of the Fermi level as in eq. (5). It has already pointed out, however, that this Fermi level is not a free parameter[33]. In a real system, in fact, the charge balance must be maintained, *i.e.* charged defects form as pairs, such as Frenkel pairs (V_{Li}^-, Li_i^+). The formation energies of V_{Li}^- and Li_i^+, calculated in eq. (5) as a function of E_F, cross at a given Fermi level and the crossing point represents their formation energies in the real system. As a consequence, the formation energies of V_{Li}^- and Li_i^+ are the same and their sum gives the formation energy of the Frenkel pair at infinite distance, i.e. for isolated defects.

Another approach can be used for computing the formation energy of defect pairs, such as Frenkel or Schottky couples. Note that the formation energy of Frenkel or Schottky pairs can be obtained from the formation energies of single defects. The formation of such couples maintains the electrical neutrality of the crystal and there is no need to add correction terms and reservoirs. Hence, formation energies are simply obtained as difference between the total energies of supercells with

View Article Online
DOI: 10.1039/D0QI00577K

and without defects. However, several possible crystallographic sites must be considered, where, for example, the interstitial atom in a Frenkel couple can move from its lattice position. Different distances between the interstitial atom and the vacancy are thus obtained and the formation energy can be obtained by extrapolation at infinite distance. Cho et al.[50] reported the results for the formation energy of Frenkel defect pairs in $LiBH_4$ using this approach.

Note that for $LiNH_2$, several theoretical values are available, and a certain scatter can be observed in **Table 3**. As different computational parameters and program codes were used, it is difficult to clearly identify possible reasons for these differences, which can be considered as differences in the experimental measurements. Note also that, in some cases,[45,49,50] a specific distance was assumed between the vacancy and the interstitial in the Frenkel couple, which may account for part of the discrepancies found.

In order to estimate the activation energy, the energies of formation for V_{Li}^- calculated in this work (**Table 3)** have been added to the calculated migration energy (**Table 1 and 3)** according to Eq. (4), and the results are reported in the last column in **Table 3**.

A comparison between computed and experimental values for the activation energy for $LiNH_2$, $LiBH_4$ and Li_2NH complex hydrides is shown in **Figure 6**. A satisfactory correspondence between theoretical and experimental values can now be observed when considering the experimental error bar. Despite the large scatter observed in both experimental and theoretical values, it appears reasonable to confirm that the Li-ion conduction mechanism theoretically considered in this work is realized in the complex hydrides.

View Article Online
DOI: 10.1039/D0QI00577K

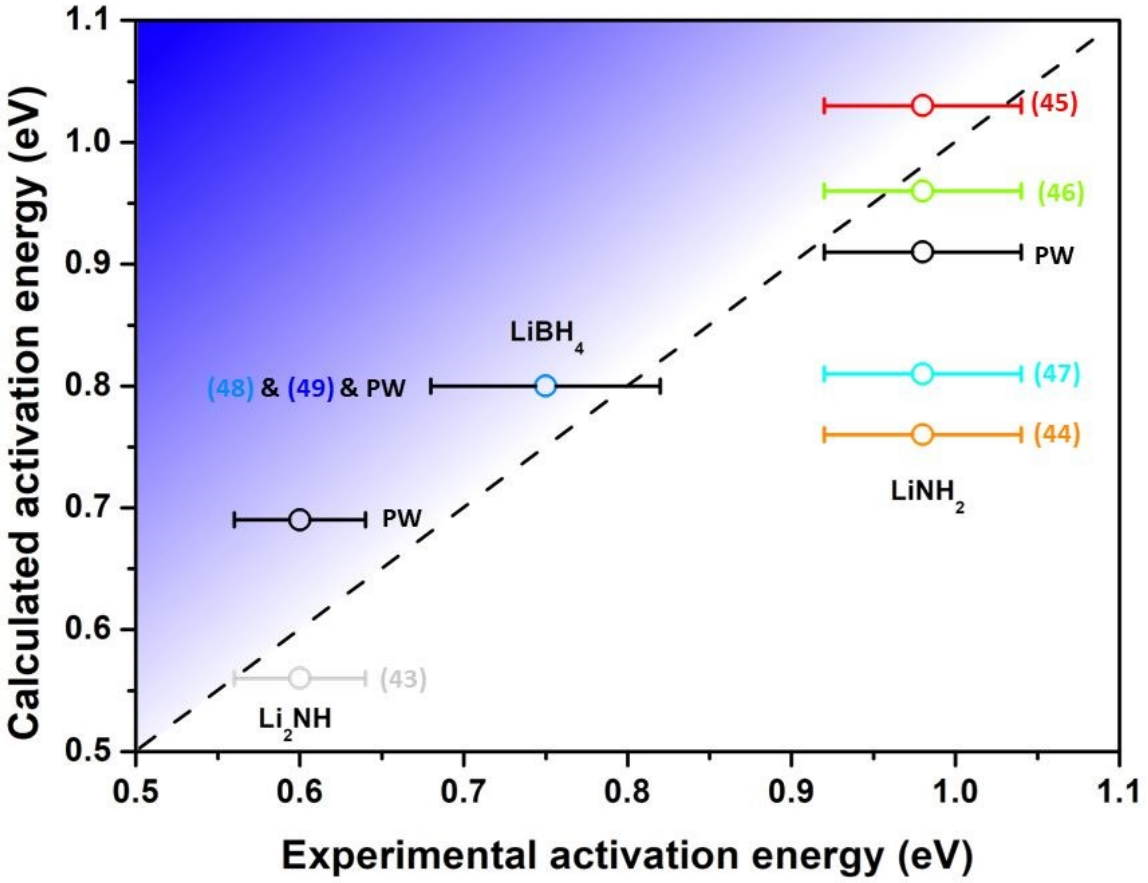

Figure 6. *Activation energy calculated as a function of the values obtained from the statistical analysis of literature data, where different colors indicates different references, PW ("present work") indicates the data calculated in this work. The dashed line is a guide for the eyes to show the correspondence of calculated and experimental values.*

4. Conclusions

We have obtained the energy limits of a certain migration map periodicities with DFT calculations by means of the NEB method for the $LiBH_4$, Li_2NH, $Li_2BH_4NH_2$, $Li_4BH_4(NH_2)_3$ and $Li_5(BH_4)_3NH$ structures. The sets of the energetically favorable migration pathways were subsequently analyzed in relation to their topologies and compared with the results of the geometrical search for migration channels. The geometrical/topological analysis of the migration pathways was performed using Voronoi partition method, which was adopted to determine cavities and channels in the structure of considered complex hydrides. It was shown that the topology of the lowest energy migration map obtained by the NEB calculations is in a good correlation with the Voronoi analysis. In addition, a statistical analysis of the literature data has been performed for each compound in order to obtain the average values for the activation energy, $\ln \sigma_0$ and Li-ion conductivity at 30 °C. A correlation

View Article Online
DOI: 10.1039/D0QI00577K

between the experimental and calculated values for Li-ion mobility has been evidenced for $LiNH_2$, $LiBH_4$ and Li_2NH complex hydrides, suggesting that the topological analysis can adequately explain the ion conductivity in complex hydrides. Authors believe that the further development of the proposed combined approach concerning other migration mechanisms or defect influence on the ionic transport properties might be of high importance for its future applications.

Acknowledgements

European Marie Curie Actions under ECOSTORE grant agreement no. 607040 is acknowledged for supporting this work. The work on the geometrical/topological analysis and DFT calculations of migration barriers was supported by the Russian Science Foundation (project 19-73-10026). We are also obliged to computational facilities of the Samara University computing complexes 'Sergey Korolev' and 'Zeolite' (Samara Center for Theoretical Materials Science).

References

(1) Pottmaier, D.; Pinatel, E. R.; Vitillo, J. G.; Garroni, S.; Orlova, M.; Baró, M. D.; Vaughan, G. B. M.; Fichtner, M.; Lohstroh, W.; Baricco, M. Structure and Thermodynamic Properties of the $NaMgH_3$ Perovskite: A Comprehensive Study. *Chem. Mater.* 2011, **23**, 2317–2326.

(2) Edwards, P. P.; Kuznetsov, V. L.; David, W. I. F.; Brandon, N. P. Hydrogen and Fuel Cells: Towards a Sustainable Energy Future. *Energy Policy* 2008, **36**, 4356–4362.

(3) Luo, X.; Wang, J.; Dooner, M.; Clarke, J. Overview of Current Development in Electrical Energy Storage Technologies and the Application Potential in Power System Operation. *Appl. Energy* 2015, **137**, 511–536.

(4) Matsuo, M.; Nakamori, Y.; Orimo, S.; Maekawa, H.; Takamura, H. Lithium Superionic Conduction in Lithium Borohydride Accompanied by Structural Transition. *Appl. Phys. Lett.* 2007, **91**, 224103.

(5) Sveinbjörnsson, D.; Christiansen, A. S.; Viskinde, R.; Norby, P.; Vegge, T. The $LiBH_4$-LiI Solid Solution as an Electrolyte in an All-Solid-State Battery. *J. Electrochem. Soc.* 2014, **161** (9), A1432–A1439.

(6) Gulino, V.; Brighi, M.; Dematteis, E. M.; Murgia, F.; Nervi, C.; Černý, R.; Baricco, M. Phase Stability and Fast Ion Conductivity in the Hexagonal $LiBH_4$–LiBr–LiCl Solid Solution. *Chem. Mater.* 2019, **31**, 5133–5144.

(7) Gulino, V.; Barberis, L.; Ngene, P.; Baricco, M.; de Jongh, P. E. Enhancing Li-Ion Conductivity in $LiBH_4$-Based Solid Electrolytes by Adding Various Nanosized Oxides. *ACS Appl. Energy Mater.* 2020, **3**, 4941–4948.

(8) Blanchard, D.; Nale, A.; Sveinbjörnsson, D.; Eggenhuisen, T. M.; Verkuijlen, M. H. W.; Suwarno; Vegge, T.; Kentgens, A. P. M.; de Jongh, P. E. Nanoconfined $LiBH_4$ as a Fast Lithium Ion Conductor. *Adv. Funct. Mater.* 2015, **25**, 184–192.

(9) Wolczyk, A.; Paik, B.; Sato, T.; Nervi, C.; Brighi, M.; GharibDoust, S. P.; Chierotti, M.; Matsuo, M.; Li, G.; Gobetto, R.; Jensen, T. R.; Černý, R.; Orimo, S.; Baricco, M. $Li_5(BH_4)_3NH$: Lithium-Rich Mixed Anion Complex Hydride. *J. Phys. Chem. C* 2017, **121**, 11069–11075.

(10) Zhou, Y.; Matsuo, M.; Miura, Y.; Takamura, H.; Maekawa, H.; Remhof, A.; Borgschulte, A.;

Zuttel, A.; Otomo, T.; Orimo, S. Enhanced Electrical Conductivities of Complex Hydrides $Li_2(BH_4)(NH_2)$ and $Li_4(BH_4)(NH_2)_3$ by Melting. *Mater. Trans.* 2011, **52**, 654–657.

(11) Matsuo, M.; Remhof, A.; Martelli, P.; Caputo, R.; Ernst, M.; Miura, Y.; Sato, T.; Oguchi, H.; Maekawa, H.; Takamura, H.; Borgschulte, A.; Züttel, A.; Orimo, S. Complex Hydrides with $(BH_4)^-$ and $(NH_2)^-$ Anions as New Lithium Fast-Ion Conductors. *J. Am. Chem. Soc.* 2009, **131**, 16389–16391.

(12) Wolczyk, A.; Pinatel, E. R.; Chierotti, M. R.; Nervi, C.; Gobetto, R.; Baricco, M. Solid-State NMR and Thermodynamic Investigations on $LiBH_4LiNH_2$ System. *Int. J. Hydrogen Energy* 2016, **41**, 14475–14483.

(13) Bölle, F. T.; Mathiesen, N. R.; Nielsen, A. J.; Vegge, T.; Garcia-Lastra, J. M.; Castelli, I. E. Autonomous Discovery of Materials for Intercalation Electrodes. *Batter. Supercaps* 2020, **3**, 488–498.

(14) Henkelman, G.; Uberuaga, B. P.; Jónsson, H. A Climbing Image Nudged Elastic Band Method for Finding Saddle Points and Minimum Energy Paths. *J. Chem. Phys.* 2000, **113**, 9901–9904.

(15) Shi, S.; Gao, J.; Liu, Y.; Zhao, Y.; Wu, Q.; Ju, W.; Ouyang, C.; Xiao, R. Multi-Scale Computation Methods: Their Applications in Lithium-Ion Battery Research and Development. *Chin. Phys. B* 2016, **25**, 018212.

(16) Deng, Z.; Zhu, Z.; Chu, I.-H.; Ong, S. P. Data-Driven First-Principles Methods for the Study and Design of Alkali Superionic Conductors. *Chem. Mater.* 2017, **29**, 281–288.

(17) Xiao, R.; Li, H.; Chen, L. Candidate Structures for Inorganic Lithium Solid-State Electrolytes Identified by High-Throughput Bond-Valence Calculations. *J. Mater.* 2015, **1**, 325–332.

(18) Anurova, N. A.; Blatov, V. A.; Ilyushin, G. D.; Blatova, O. A.; Ivanov-Schitz, A. K.; Dem'yanets, L. N. Migration Maps of Li^+ cations in Oxygen-Containing Compounds. *Solid State Ionics* 2008, **179**, 2248–2254.

(19) Meutzner, F.; Münchgesang, W.; Kabanova, N. A.; Zschornak, M.; Leisegang, T.; Blatov, V. A.; Meyer, D. C. On the Way to New Possible Na-Ion Conductors: The Voronoi-Dirichlet Approach, Data Mining and Symmetry Considerations in Ternary Na Oxides. *Chem. - A Eur. J.* 2015, **21**, 16601–16608.

(20) Brighi, M.; Schouwink, P.; Sadikin, Y.; Černý, R. Fast Ion Conduction in Garnet-Type Metal Borohydrides $Li_3K_3Ce_2(BH_4)_{12}$ and $Li_3K_3La_2(BH_4)_{12}$. *J. Alloys Compd.* 2016, **662**, 388–395.

(21) Blatov, V. A.; Shevchenko, A. P.; Proserpio, D. M. Applied Topological Analysis of Crystal Structures with the Program Package ToposPro. *Cryst. Growth Des.* 2014, **14**, 3576–3586.

(22) GharibDoust, S. H. P.; Brighi, M.; Sadikin, Y.; Ravnsbæk, D. B.; Černý, R.; Skibsted, J.; Jensen, T. R. Synthesis, Structure, and Li-Ion Conductivity of $LiLa(BH_4)_3X$, X = Cl, Br, I. *J. Phys. Chem. C* 2017, **121**, 19010–19021.

(23) Didelot, E.; Černý, R. Ionic Conduction in Bimetallic Borohydride Borate, $LiCa_3(BH_4)(BO_3)_2$. *Solid State Ionics* 2017, **305**, 16–22.

(24) Franco, F.; Baricco, M.; Chierotti, M. R.; Gobetto, R.; Nervi, C. Coupling Solid-State NMR with GIPAW Ab Initio Calculations in Metal Hydrides and Borohydrides. *J. Phys. Chem. C* 2013, **117**, 9991–9998.

(25) Eremin, R. A.; Kabanova, N. A.; Morkhova, Y. A.; Golov, A. A.; Blatov, V. A. High-Throughput Search for Potential Potassium Ion Conductors: A Combination of Geometrical-Topological and Density Functional Theory Approaches. *Solid State Ionics* 2018, **326**, 188–199.

(26) Eremin, R. A.; Zolotarev, P. N.; Golov, A. A.; Nekrasova, N. A.; Leisegang, T. Ionic Transport in Doped Solid Electrolytes by Means of DFT Modeling and ML Approaches: A Case Study of Ti-Doped $KFeO_2$. *J. Phys. Chem. C* 2019, 123, 29533–29542.

(27) Perdew, J. P.; Burke, K.; Ernzerhof, M. Generalized Gradient Approximation Made Simple. *Phys. Rev. Lett.* 1996, **77**, 3865–3868.

(28) Kresse, G.; Furthmüller, J. Efficient Iterative Schemes for Ab Initio Total-Energy Calculations Using a Plane-Wave Basis Set. *Phys. Rev. B* 1996, **54**, 11169–11186.

(29) Hutter, J.; Iannuzzi, M.; Schiffmann, F.; VandeVondele, J. CP2K: Atomistic Simulations of Condensed Matter Systems. *Wiley Interdiscip. Rev. Comput. Mol. Sci.* 2014, **4**, 15–25.

(30) VandeVondele, J.; Krack, M.; Mohamed, F.; Parrinello, M.; Chassaing, T.; Hutter, J. Quickstep: Fast and Accurate Density Functional Calculations Using a Mixed Gaussian and Plane Waves Approach. *Comput. Phys. Commun.* 2005, **167**, 103–128.

(31) Goodenough, J. B. Review Lecture: Fast Ionic Conduction in Solids. *Proc. R. Soc. A Math.*

View Article Online
DOI: 10.1039/D0QI00577K

Phys. Eng. Sci. 1984, **393**, 215–234.

(32) Goodenough, J. B. Oxide-Ion Electrolytes. *Annu. Rev. Mater. Res.* 2003, **33**, 91–128.

(33) Van de Walle, C. G.; Neugebauer, J. First-Principles Calculations for Defects and Impurities: Applications to III-Nitrides. *J. Appl. Phys.* 2004, **95**, 3851–3879.

(34) Van de Walle, C. G.; Denteneer, P. J. H.; Bar-Yam, Y.; Pantelides, S. T. Theory of Hydrogen Diffusion and Reactions in Crystalline Silicon. *Phys. Rev. B* 1989, **39**, 10791–10808.

(35) Slater, J. C. Atomic Radii in Crystals. *J. Chem. Phys.* 1964, **41**, 3199–3204.

(36) Blatov, V. A.; O'Keeffe, M.; Proserpio, D. M. Vertex-, Face-, Point-, Schläfli-, and Delaney-Symbols in Nets, Polyhedra and Tilings: Recommended Terminology. *CrystEngComm* 2010, **12**, 44–48.

(37) Koch. E.; Fischer, W. Z. Types of Sphere Packings for Crystallographic Point Groups, Rod Groups and Layer Groups. *K. Krist.* 1978, **148**, 107–152.

(38) O'Keeffe, M.; Peskov, M. A.; Ramsden, S. J.; Yaghi, O. M. The Reticular Chemistry Structure Resource (RCSR) Database of, and Symbols for, Crystal Nets. *Acc. Chem. Res.* 2008, **41**, 1782–1789.

(39) Blatov, V. A.; Alexandrov, E. V.; Shevchenko, A. P. Topology: ToposPro. In *Reference Module in Chemistry, Molecular Sciences and Chemical Engineering*; Elsevier, 2019, 1–23.

(40) Matsuo, M.; Takamura, H.; Maekawa, H.; Li, H.-W.; Orimo, S. Stabilization of Lithium Superionic Conduction Phase and Enhancement of Conductivity of $LiBH_4$ by LiCl Addition. *Appl. Phys. Lett.* 2009, **94**, 084103.

(41) Sveinbjörnsson, D.; Blanchard, D.; Myrdal, J. S. G.; Younesi, R.; Viskinde, R.; Riktor, M. D.; Norby, P.; Vegge, T. Ionic Conductivity and the Formation of Cubic CaH2 in the $LiBH_4$–$Ca(BH_4)_2$ Composite. *J. Solid State Chem.* 2014, **211**, 81–89.

(42) Martelli, P.; Remhof, A.; Borgschulte, A.; Ackermann, R.; Strässle, T.; Embs, J. P.; Ernst, M.; Matsuo, M.; Orimo, S.-I.; Züttel, A. Rotational Motion in $LiBH_4$/LiI Solid Solutions. *J. Phys. Chem. A* 2011, **115**, 5329–5334.

(43) Jansen, M. Volume Effect or Paddle-Wheel Mechanism—Fast Alkali-Metal Ionic Conduction in Solids with Rotationally Disordered Complex Anions. *Angew. Chemie Int. Ed.*

View Article Online
DOI: 10.1039/D0QI00577K

English 1991, **30**, 1547–1558.

(44) Li, W.; Wu, G.; Xiong, Z.; Feng, Y. P.; Chen, P. Li^+ Ionic Conductivities and Diffusion Mechanisms in Li-Based Imides and Lithium Amide. *Phys. Chem. Chem. Phys.* 2012, **14**, 1596–1606.

(45) Hoang, K.; Janotti, A.; Van De Walle, C. G. The Particle-Size Dependence of the Activation Energy for Decomposition of Lithium Amide. *Angew. Chemie - Int. Ed.* 2011, **50**, 10170–10173.

(46) Hazrati, E.; Brocks, G.; Buurman, B.; De Groot, R. A.; De Wijs, G. A. Intrinsic Defects and Dopants in $LiNH_2$: A First-Principles Study. *Phys. Chem. Chem. Phys.* 2011, **13**, 6043–6052.

(47) Wang, J.; Du, Y.; Xu, H.; Jiang, C.; Kong, Y.; Sun, L.; Liu, Z. K. Native Defects in $LiNH_2$: A First-Principles Study. *Phys. Rev. B - Condens. Matter Mater. Phys.* 2011, **84**, 21–24.

(48) Miceli, G.; Cucinotta, C. S.; Bernasconi, M.; Parrinello, M. First Principles Study of the $LiNH_2$/Li_2NH Transformation. *J. Phys. Chem. C* 2010, **114**, 15174–15183.

(49) Hoang, K.; Van De Walle, C. G. Mechanism for the Decomposition of Lithium Borohydride. *Int. J. Hydrogen Energy* 2012, **37**, 5825–5832.

(50) Lee, Y.-S.; Cho, Y. W. Fast Lithium Ion Migration in Room Temperature $LiBH_4$. *J. Phys. Chem. C* 2017, **121**, 17773–17779.

Graphical Abstract

View Article Online
DOI: 10.1039/D0QI00577K

Highlights

- The topological analysis of crystal structures for various complex hydrides has been performed with the ToposPro program package and possible migration energy limits have been calculated by DFT.
- The activation energies for the Li^+ ion migration have been determined by the statistical analysis of the literature data.
- A correlation between computed and experimental activation energies has been evidenced for the $LiNH_2$, $LiBH_4$ and Li_2NH compounds, suggesting that the topological analysis can adequately explain the ion conductivity in complex hydrides.

Competing interest statement

Authors have no competing interests to declare.

Electronic Supplementary Material (ESI) for Inorganic Chemistry Frontiers.

Combined DFT and Geometrical-Topological Analysis of Li-ion conductivity in Complex Hydrides

Valerio Gulino[1#], Anna Wolczyk[1#], Andrey A. Golov[2], Roman A. Eremin[2,3], Mauro Palumbo[1], Carlo Nervi[1], Vladislav A. Blatov[2,3*], Davide M. Proserpio[3,4] and Marcello Baricco[1]*

[1]Department of Chemistry and NIS, University of Turin, Via P. Giuria 9, I-10125 Torino, Italy
[2]Samara Center for Theoretical Materials Science, Samara University, Samara 443011, Russia
[3]Samara Center for Theoretical Materials Science, Samara State Technical University, Samara 443100, Russia
[4]Dipartimento di Chimica, Università degli studi di Milano, 20133, Milano, Italy

[#]co-first authors

[*]Corresponding authors:
Prof. Mauro PALUMBO
Department of Chemistry, University of Turin
Via Pietro Giuria, 9 I-10125 TORINO (Italy)
Tel. + 39 011 670 7097 Fax. + 39 011 670 7855
e-mail: mauro.palumbo@unito.it

Prof. Vladislav A. BLATOV
Samara Center for Theoretical Materials Science, Samara State Technical University
Samara 443100, Russia
Tel. +7 846 3356798 Fax: +7 846 2784400
e-mail: blatov@topospro.com

Supporting information

Crystal structure of investigated complex hydrides

Sample	Space Group	Lattice constants (Å)	Ref.
$LiBH_4$	*Pnma*	*a* = 7.178 Å *b* = 6.803 Å *c* = 4.436 Å	1
Li_2NH	*Fm3m*	*a* = 5.074	2
$LiNH_2$	*I-4*	*a* = 5.079 *c* = 10.113	3
$Li_2BH_4NH_2$	*R-3*	*a* = 14.498 *c* = 9.248	4
$Li_4BH_4(NH_2)_3$	$I2_13$	*a* = 10.673	4
$Li_5(BH_4)_3NH$	*Pnma*	*a* = 10.203, *b* = 11.501 *c* = 7.047	5

Table S1. *Structural details of all considered samples.*

Topological analysis

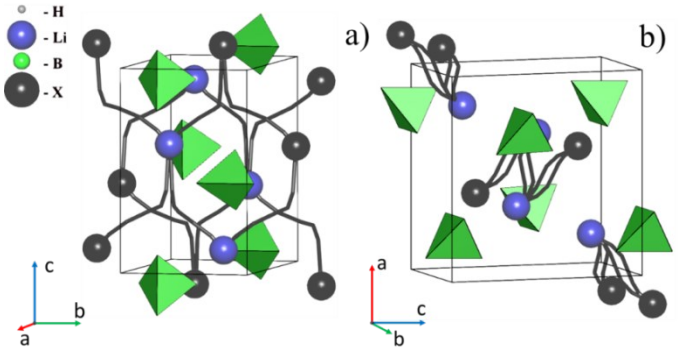

Figure S1. *The lowest energy Li^+ migration pathways in the $LiBH_4$ structure. The migration energies of the pathways: a) 0.242; b) 0.298 eV. Hereafter the points labeled as X correspond to equilibrium Li positions and are linked by the NEB trajectories.*

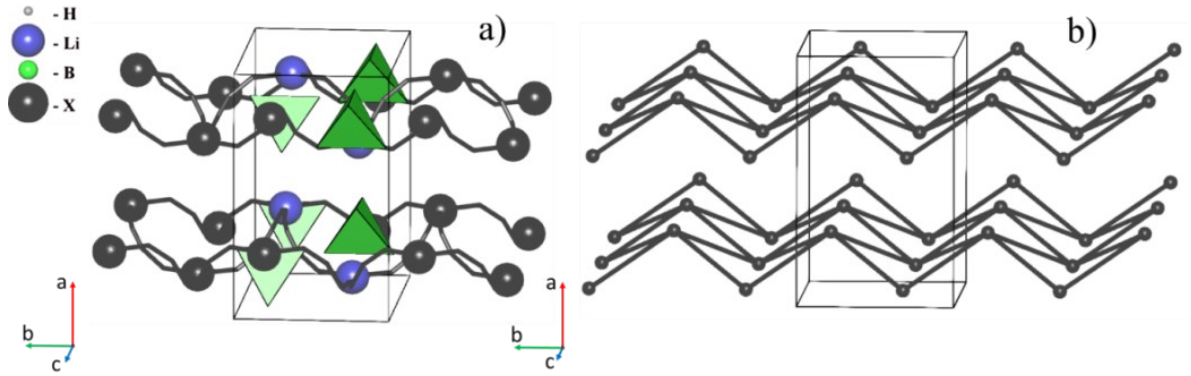

Figure S2. *a) The lowest energy two-periodic Li^+ migration map in the $LiBH_4$ structure, b) the simplified migration map of the sql topology.*

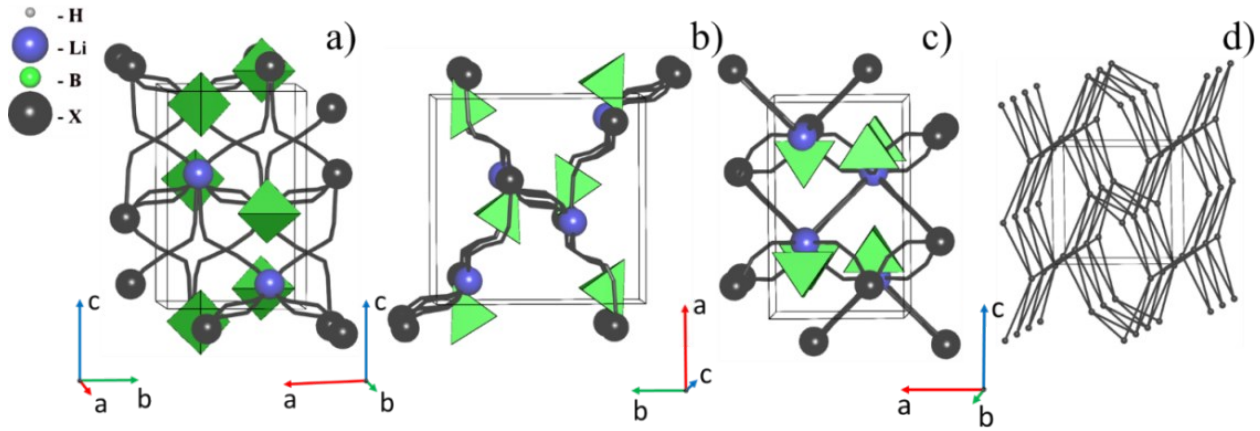

Figure S3. *a)-c) The lowest energy three-periodic Li^+ migration map in the $LiBH_4$ structure, d) the simplified migration map of the acs topology.*

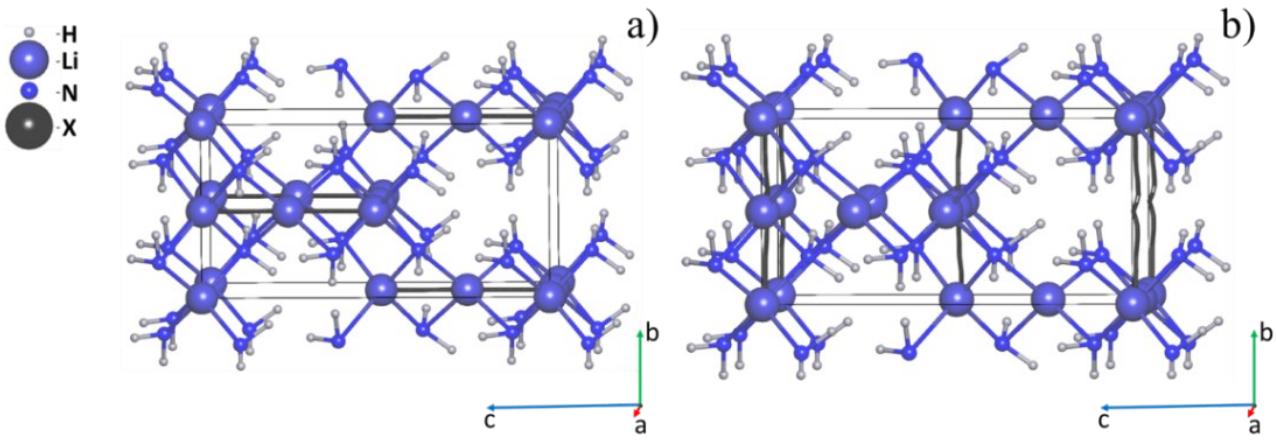

Figure S4. *The lowest energy Li^+ migration pathways in the structure $LiNH_2$. The migration energies of the pathways: a) 0.179; b) 0.461 eV.*

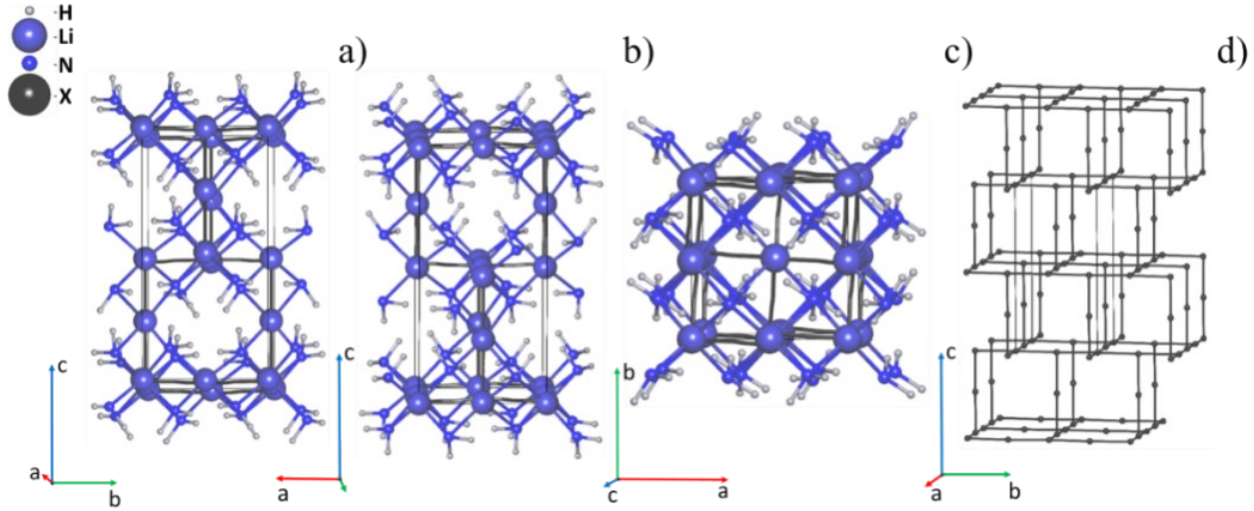

Figure S5. *a)-c) The lowest energy three-periodic Li^+ migration map in the $LiNH_2$ structure, d) the simplified migration map of the tfa topology.*

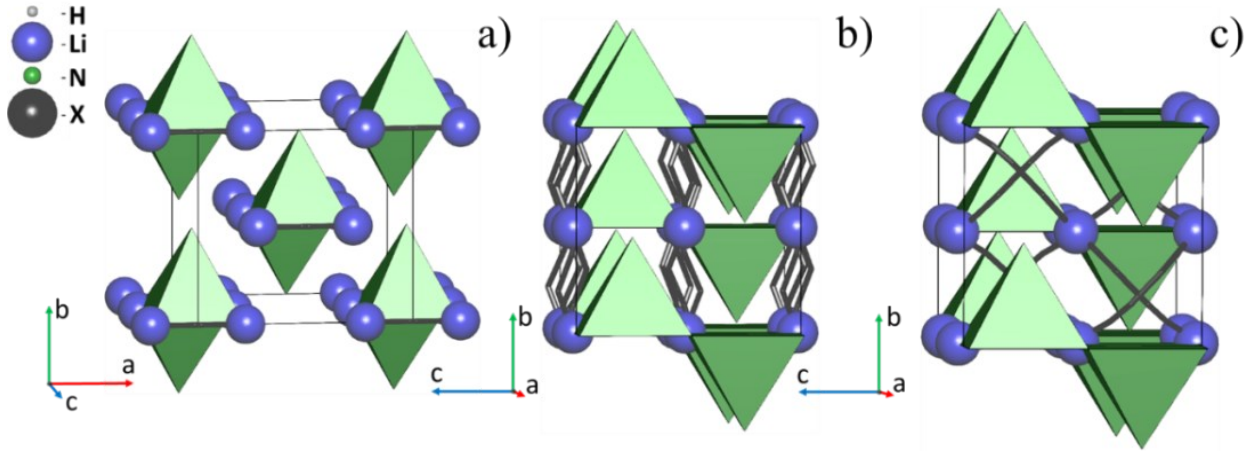

Figure S6. *The lowest energy Li^+ migration pathways in the Li_2NH structure. The migration energies of the pathways: a) 0.007; b) 0.308; c) 0.321 eV.*

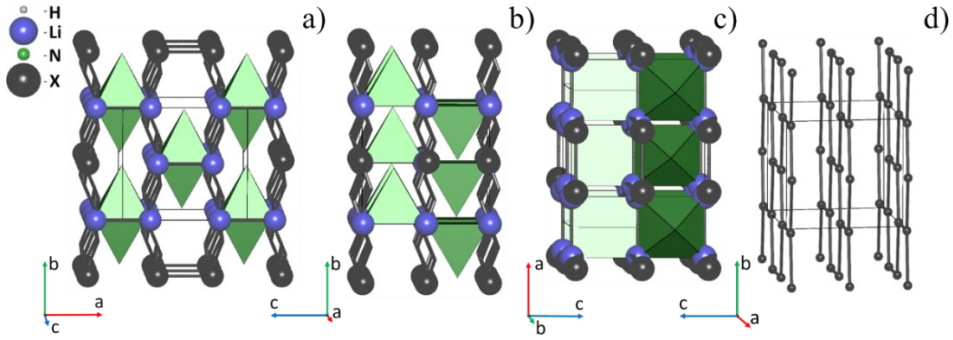

Figure S7. *a)-c) The lowest energy two-periodic Li^+ migration map in the Li_2NH structure, d) the simplified migration map of the hcb topology.*

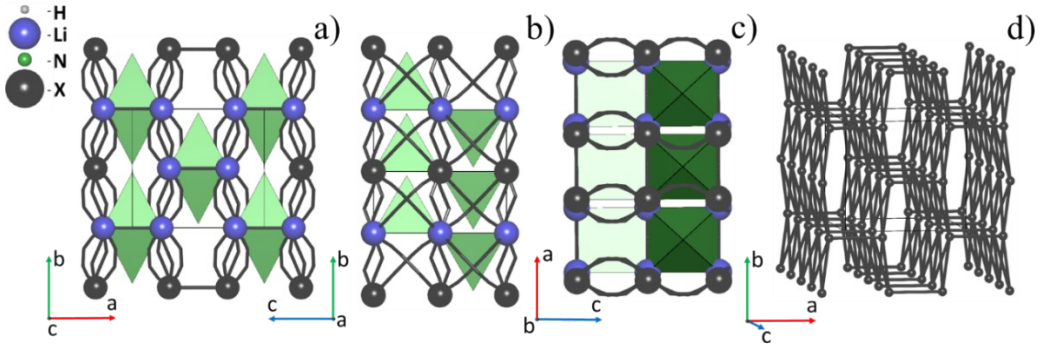

Figure S8. *a)-c) The lowest energy three-periodic Li^+ migration map in the Li_2NH structure, d) the simplified migration map of the sqc2-7-Cmmm topology.*

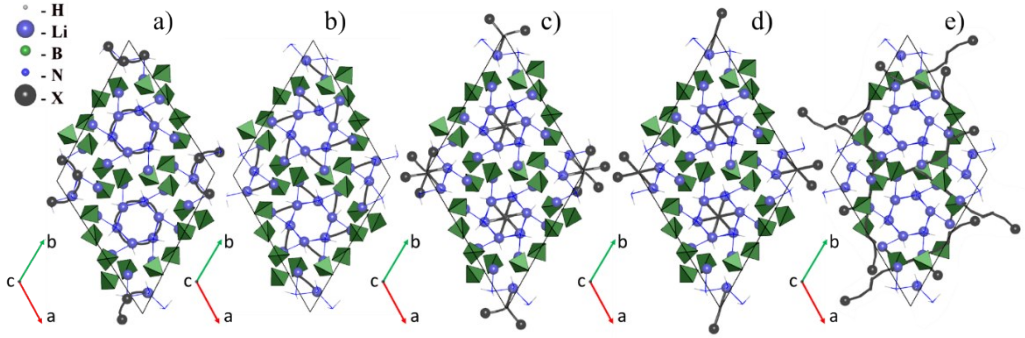

Figure S9. *The lowest energy Li^+ migration pathways in the $Li_2BH_4NH_2$ structure. The migration energies of the pathways: a) 0.176; b) 0.365; c) 0.445; d) 0.481; e) 0.525 eV.*

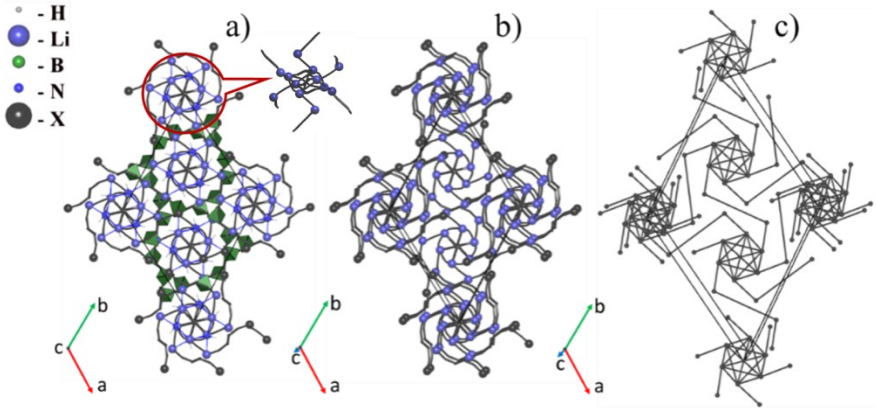

Figure S10. *a), b) The lowest energy three-periodic 2-fold interpenetrated Li^+ migration map in the $Li_2BH_4NH_2$ structure, c) the simplified migration map.*

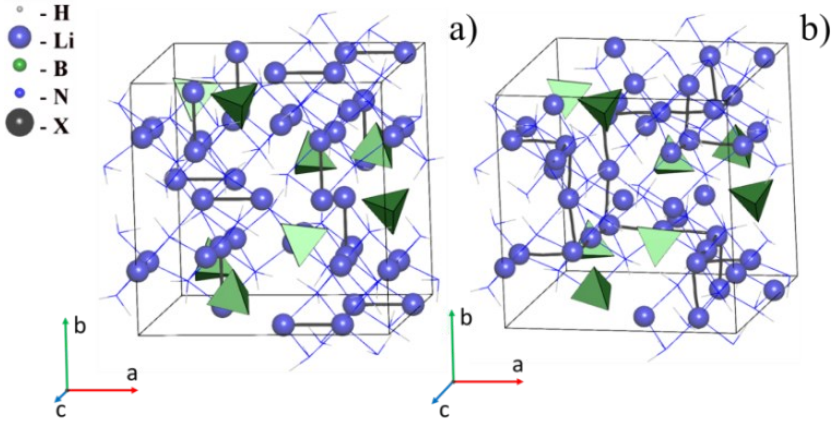

Figure S11. *The lowest energy Li^+ migration pathways in the $Li_4BH_4(NH_2)_3$ structure. The migration energy of the pathways: a) 0.212; b) 0.296 eV.*

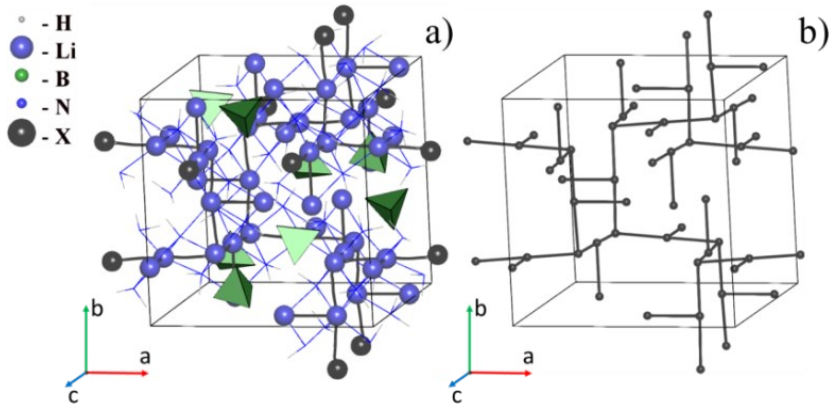

Figure S12. *a) The lowest energy three-periodic Li^+ migration map in the structure $Li_4BH_4(NH_2)_3$, b) the simplified migration map of the srs topology.*

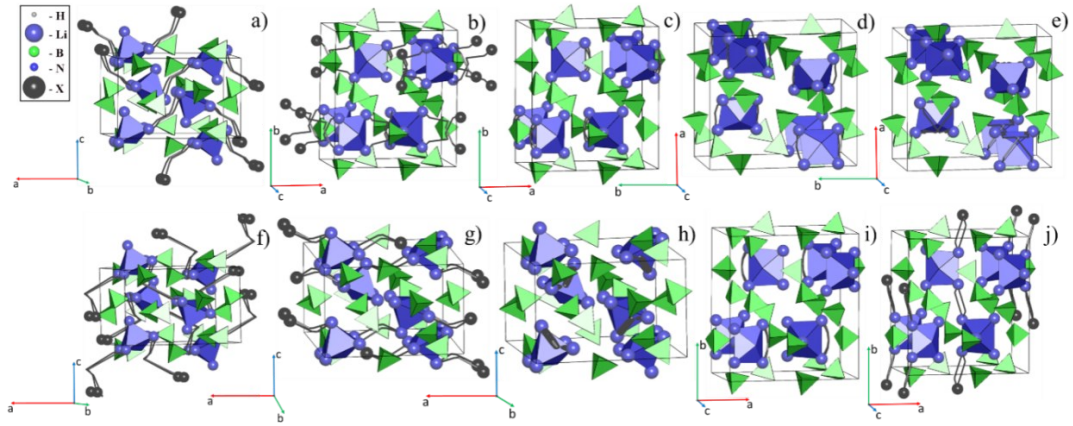

Figure S13. *The lowest energy Li^+ migration pathways in the $Li_5(BH_4)_3NH$ structure. The migration energies of the pathways: a) 0.237; b) 0.282; c) 0.340; d) 0.397; e) 0.401; f) 0.479; g) 0.536; h) 0.541; i) 0.547; j) 0.559 eV.*

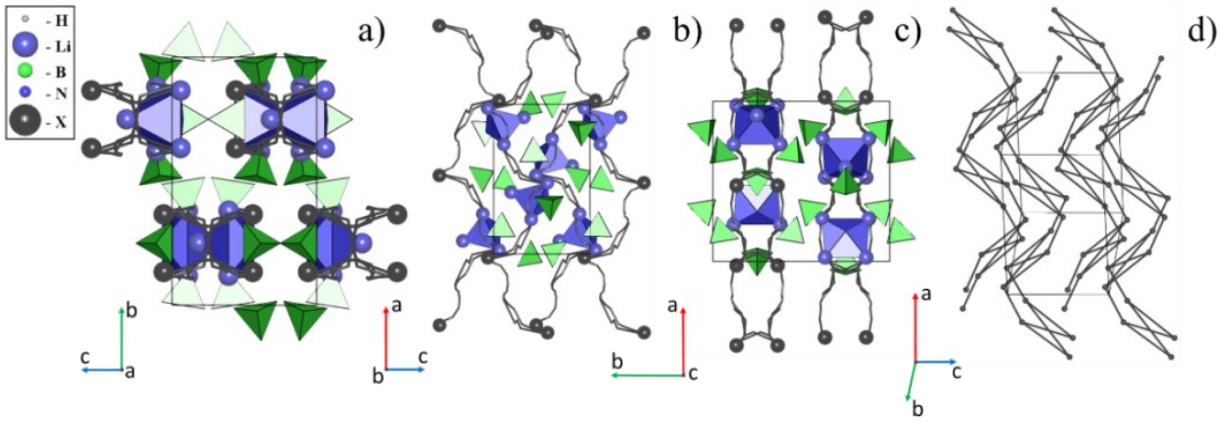

Figure S14. *a)-c) The lowest energy one-periodic Li^+ migration map in the $Li_5(BH_4)_3NH$ structure, d) the simplified migration map of the $6^3(0,2)$ topology.*

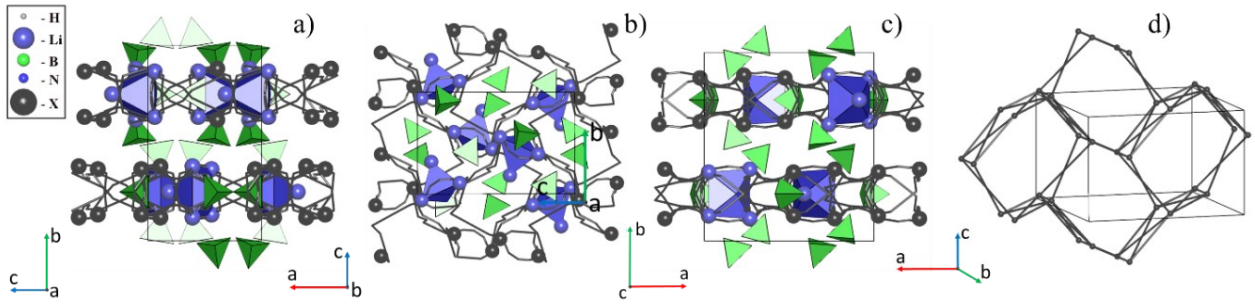

Figure S15. *a)-c) The lowest energy two-periodic Li^+ migration map in the $Li_5(BH_4)_3NH$ structure, d) the simplified migration map with an unknown topology.*

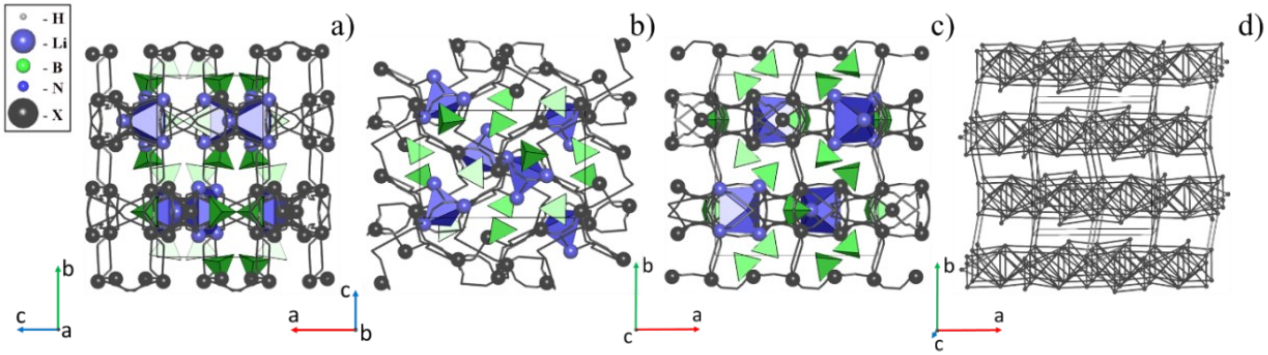

Figure S16. *a)-c) The lowest energy three-periodic Li^+ migration map in the $Li_5(BH_4)_3NH$ structure, d) the simplified migration map with an unknown topology.*

Statistical analysis of literature data of Li-ion conductivity in $LiBH_4$

A statistical analysis was performed in order to obtain the average value of activation energy (E_A), $\ln\sigma_0$ and Li-ion conductivity at room temperature for $LiBH_4$, using literature data.[6–14] Only data related to the orthorhombic phase stable at room temperature have been considered.

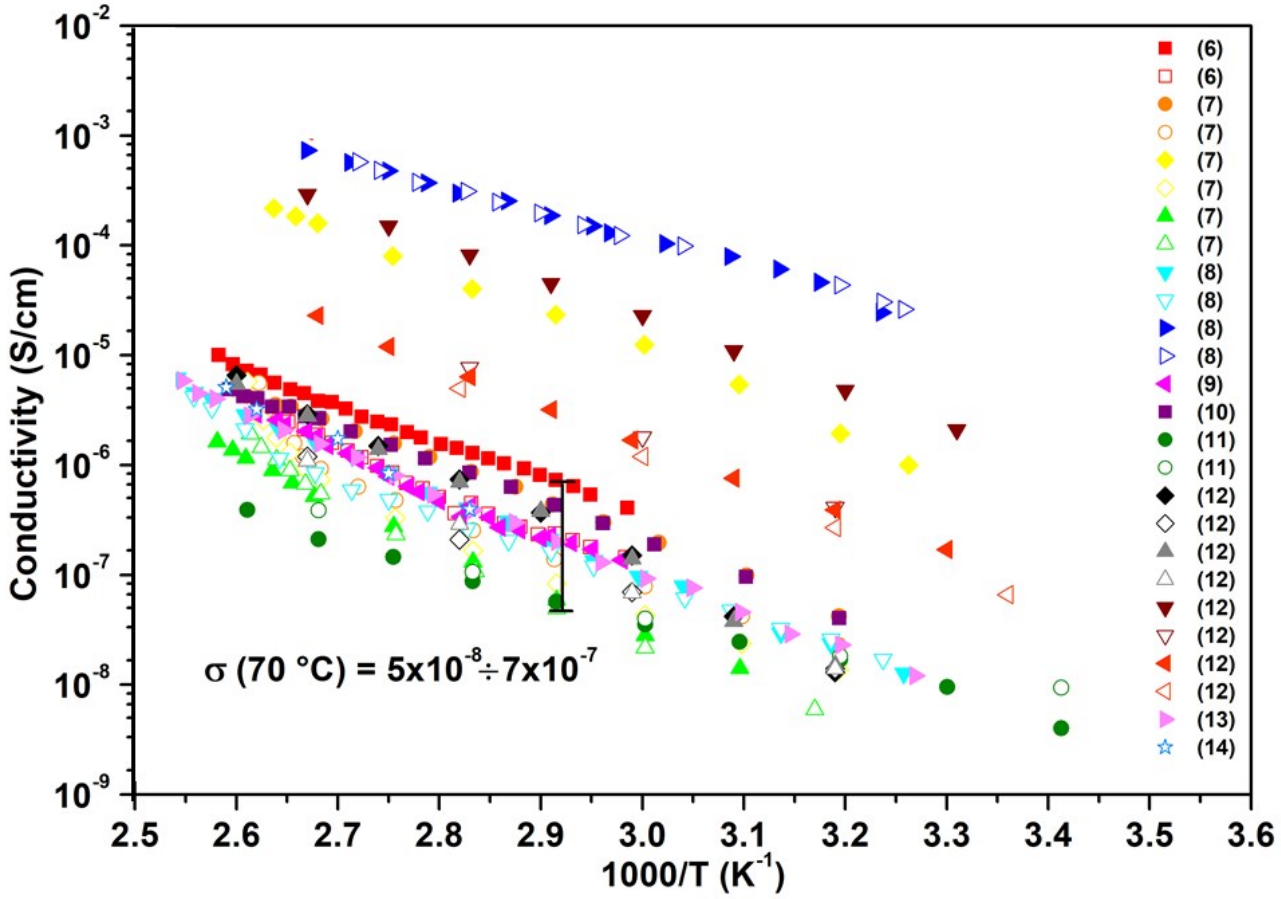

Figure S17. *Li-ion conductivity data for orthorhombic $LiBH_4$ reported in literature. Full and empty symbols refer to the heating and cooling temperature-dependent EIS ramp, respectively. The error bar for the Li-ion conductivity at 70 °C is indicated as an example.*

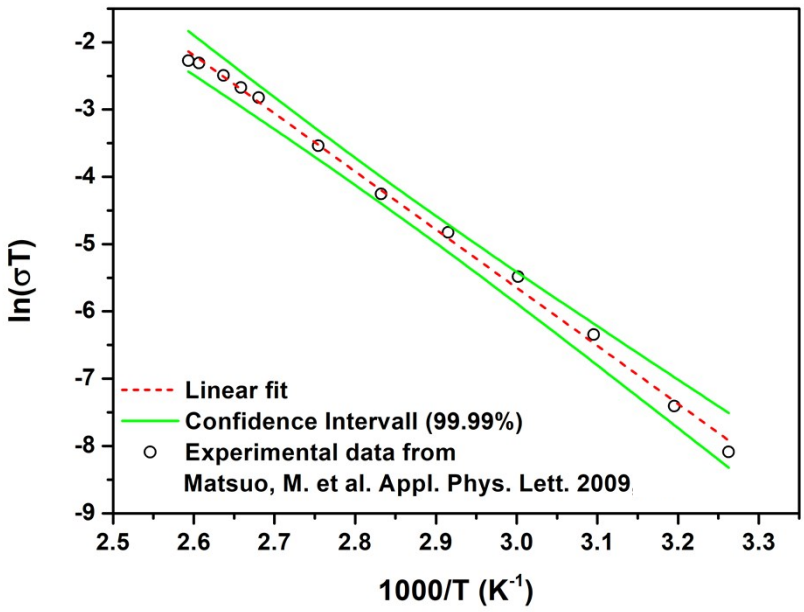

Figure S18. *Example of linear fit on Li-ion conductivity for the orthorombic phase of $LiBH_4$ as a function of inverse temperature. Data form Matsuo, M. et al. Appl. Phys. Lett.* ***2009****, 94, 224103 (Ref. 6).*

Temperature-dependent EIS ramp	Temperature-dependent EIS cycle	Milled	E_A (eV)	C.I.	Ref.
Heating	1st	No	0.69	0.04	(1)
Cooling	1st	No	0.81	0.09	(1)
Heating	1st	No	0.71	0.04	(2)
Cooling	1st	No	0.7	0.1	(2)
Heating	1st	**Yes**	**0.74**	**0.07**	(2)
Cooling	1st	**Yes**	**0.7**	**0.3**	(2)
Heating	2nd	**Yes**	**0.8**	**0.1**	(2)
Cooling	2nd	**Yes**	**0.9**	**0.2**	(3)
Heating	1st	No	0.77	0.04	(3)
Cooling	1st	No	0.7	0.1	(3)
Heating	1st	**Yes**	**0.51**	**0.07**	(3)
Cooling	1st	**Yes**	**0.51**	**0.05**	(3)
Heating	1st	No	0.8	0.1	(4)
Heating	1st	No	0.71	0.04	(5)
Heating	1st	No	0.50	0.1	(6)
Heating	1st	No	0.91	0.08	(7)
Heating	2nd	No	0.89	0.06	(7)
Heating	1st	**Yes**	**0.70**	**0.03**	(7)
Heating	2nd	**Yes**	**0.75**	**0.04**	(7)
Heating	1st	No	0.76	0.04	(8)
Average			**0.73**	**0.08**	
Average exclude bold data			**0.75**	**0.07**	

Table S2. *Activation energy (eV) calculated by linear plot of ln(σT) and 1000/T of literature data, for $LiBH_4$ (99.99 % of confidence). CI is the confidence interval half width. The bold (red) data were excluded in the second calculation of the average activation energy data. 1st and 2nd refers to the temperature-dependent EIS cycle data.*

Temperature-dependent EIS ramp	Temperature-dependent EIS cycle	Milled	$\ln\sigma_0$	C.I.	Ref.
Heating	1st	No	15	1	(1)
Cooling	1st	No	18	3	(1)
Heating	1st	No	15	1	(2)
Cooling	1st	No	13	5	(2)
Heating	1st	**Yes**	**20**	**2**	(2)
Cooling	1st	**Yes**	**14**	**10**	(2)
Heating	2nd	**Yes**	**17**	**3**	(2)
Cooling	2nd	**Yes**	**20**	**8**	(3)
Heating	1st	No	16	1	(3)
Cooling	1st	No	14	4	(3)
Heating	1st	**Yes**	**15**	**2**	(3)
Cooling	1st	**Yes**	**14**	**2**	(3)
Heating	1st	No	18	3	(4)
Heating	1st	No	15	1	(5)
Heating	1st	No	6	4	(6)
Heating	1st	No	21	2	(7)
Heating	2nd	No	22	2	(7)
Heating	1st	**Yes**	**19.3**	**0.3**	(7)
Heating	2nd	**Yes**	**17**	**1**	(7)
Heating	1st	No	16	1	(8)
Average			**16**	**3**	
Average exclude bold data			**16**	**2**	

Table S3. *$\ln\sigma_0$ calculated by linear plot of $\ln(\sigma T)$ and 1000/T of literature data, for $LiBH_4$ (99.99 % of confidence). CI is the confidence interval half width. The bold (red) data were excluded in the second calculation of the average $\ln\sigma_0$. 1st and 2nd refers to the temperature-dependent EIS cycle data.*

Temperature-dependent EIS ramp	Temperature-dependent EIS cycle	Milled	$\ln(\sigma T)_{FIT}$	$\ln(\sigma T)_{MAX}$	$\ln(\sigma T)_{MIN}$	Ref.
Heating	1st	No	-11.40	-11.18	-11.63	(1)
Cooling	1st	No	-13.12	-12.59	-13.66	(1)
Heating	1st	No	-11.98	-11.78	-12.19	(2)
Cooling	1st	No	-12.78	-13.93	-11.63	(2)
Heating	1st	**Yes**	**-8.23**	**-7.85**	**-8.61**	(2)
Cooling	1st	**Yes**	**-13.48**	**-12.12**	**-14.84**	(2)
Heating	2nd	**Yes**	**-14.41**	**-13.80**	**-15.02**	(2)
Cooling	2nd	**Yes**	**-14.90**	**-13.49**	**-16.30**	(3)
Heating	1st	No	-12.95	-12.74	-13.16	(3)
Cooling	1st	No	-12.83	-12.23	-13.43	(3)
Heating	1st	**Yes**	**-5.04**	**-4.77**	**-5.31**	(3)
Cooling	1st	**Yes**	**-5.01**	**-4.82**	**-5.20**	(3)
Heating	1st	No	-13.17	-12.53	-13.81	(4)
Heating	1st	No	-12.01	-11.81	-12.21	(5)
Heating	1st	No	-12.90	-12.53	-13.26	(6)
Heating	1st	No	-13.31	-13.04	-13.58	(7)
Heating	2nd	No	-13.72	-13.44	-13.99	(7)
Heating	1st	**Yes**	**-7.25**	**-6.36**	**-8.13**	(7)
Heating	2nd	**Yes**	**-11.81**	**-11.24**	**-12.37**	(7)
Heating	1st	No	-12.90	-12.68	-13.12	(8)
Average $\ln(\sigma T)$			**-11.66**	**-11.25**	**-12.07**	**C.I.**
Average σ at 30 °C			**2.85×10^{-8}**	**4.30×10^{-8}**	**1.89×10^{-8}**	**1.21×10^{-8}**
Average $\ln(\sigma T)$ exclude bold data			**-12.76**	**-12,54**	**-12,97**	**C.I.**
Average σ at 30 °C exclude bold data			**9.5×10^{-9}**	**1.18×10^{-8}**	**7.66×10^{-9}**	**2.07×10^{-9}**

Table S4. *ln(σT) and Li-ion conductivity at 30 °C (303.14 K) calculated using the data (1000 E_A/k_B and $\ln\sigma_0$) obtained by the linear plot of ln(σT) and 1000/T of literature data (see Table S1 and Table S2) for $LiBH_4$. $\ln(\sigma T)_{FIT}$ has been calculated using the slope and intercept obtained by the linear fit. $\ln(\sigma T)_{MAX}$ and $\ln(\sigma T)_{MIN}$ were calculated considering the maximum and the minimum values, of the slope and intercept, of confidence interval obtained by the linear fit. The bold (red) data were excluded in the second calculation of the average ln(σT) data. 1st and 2nd refers to the temperature-dependent EIS cycle data. CI is the confidence interval half width, calculated averaging the $\ln(\sigma T)_{MAX}$ and the $\ln(\sigma T)_{MIN}$.*

Statistical analysis for $LiNH_2$, Li_2NH, $Li_2(NH_2)(BH_4)$ and $Li_4(NH_2)_3(BH_4)$

Statistical analysis was performed in order to obtain the average value of activation energy for $LiNH_2$, Li_2NH, $Li_2(NH_2)(BH_4)$ and $Li_4(NH_2)_3(BH_4)$, using the data reported in literature.[10,15–18]

Compound	Temperature-dependent EIS ramp	Temperature-dependent EIS cycle	E_A	C.I.	$\ln\sigma_0$	C.I.	Ref.
$LiNH_2$	Heating	1st	0.9	0.04	19	1	(10)
	Heating	1st	1.05	0.08	19	2	(11)
	Average		**0.98**	**0.06**	**19**	**2**	
Li_2NH	Heating	1st	0.63	0.01	21.8	0.2	(11)
	Heating	1st	0.58	0.02	20,1	0,9	(12)
	Heating	1st	0.6	0.1	20	5	(12)
	Average		**0.60**	**0.04**	**21**	**2**	
$Li_2NH_2BH_4$	Heating	1st	0.7	0.04	23	1	(10)
	Cooling	1st	0.67	0.06	22	2	(10)
	Average		**0.69**	**0.06**	**23**	**2**	
$Li_4(NH_2)_3BH_4$	Heating	1st	0.26	0.01	7,0	0,4	(5)
	Heating	1st	0.33	0.01	8.7	0.4	(10)
	Cooling	1st	0.55	0.03	13	1	(10)
	Heating	1st	0.34	0.01	11	1	(13)
	Average		**0.37**	**0.02**	**10.1**	**0.6**	

Table S5. *Activation energy (eV) and $\ln\sigma_0$ calculated by linear plot of $\ln(\sigma T)$ and 1000/T of literature data, for the $LiNH_2$, Li_2NH, $Li_2(NH_2)(BH_4)$ and $Li_4(NH_2)_3(BH_4)$ (95 % of confidence). CI is the confidence interval half width.*

Compound	Temperature-dependent EIS ramp	Temperature-dependent EIS cycle	$\ln(\sigma T)_{FIT}$	$\ln(\sigma T)_{MAX}$	$\ln(\sigma T)_{MIN}$	Ref.
$LiNH_2$	Heating	1st	-14.97	-14.71	-15.23	(5)(10)
	Heating	1st	-20.90	-19.75	-22.05	(11)
	Average $\ln(\sigma T)$		**-17.94**	**-17.23**	**-18.64**	**C.I.**
	Average σ at 30 °C		**$5.36x10^{-11}$**	**$1.09x10^{-10}$**	**$2.64x10^{-11}$**	**$4.11x10^{-11}$**
Li_2NH	Heating	1st	-2.41	-2,38	-2,44	11
	Heating	1st	-2.22	-2,17	-2,27	12
	Heating	1st	-1.96	-1,32	-2,61	12
	Average $\ln(\sigma T)$		**-2.20**	**-1,96**	**-2,44**	**C.I.**
	Average σ at 30 °C		**$3.66x10^{-4}$**	**$4.66x10^{-4}$**	**$2.88x10^{-4}$**	**$8.92x10^{-5}$**
$Li_2NH_2BH_4$	Heating	1st	-3.36	-3.22	-3.50	(5)(10)
	Cooling	1st	-3.62	-3.43	-3.80	(10)
	Average $\ln(\sigma T)$		**-3.49**	**-3.33**	**-3.65**	**C.I.**
	Average σ at 30 °C		**$1.01x10^{-4}$**	**$1.18x10^{-4}$**	**$8.57x10^{-5}$**	**$1.63x10^{-5}$**
$Li_4(NH_2)_3BH_4$	Heating	1st	-2.93	-2.86	-3.00	(5)
	Heating	1st	-3.53	-3.44	-3.62	(10)
	Cooling	**1st**	**-7.59**	**-7.39**	**-7.79**	(10)
	Heating	1st	-2.74	-2.11	-3.37	(13)
	Average $\ln(\sigma T)$		**-4.19**	**-3.95**	**-4.44**	**C.I.**
	Average σ at 30 °C		**$4.98x10^{-5}$**	**$6.37x10^{-5}$**	**$3.89x10^{-5}$**	**$1.24x10^{-5}$**
	Average $\ln(\sigma T)$ exclude bold data		**-3,06**	**-2.80**	**-3.33**	**C.I.**
	Average σ at 30 °C exclude bold data		**$1.54x10^{-4}$**	**$2.00x10^{-4}$**	**$1.14x10^{-4}$**	**$4.09x10^{-5}$**

Table S6. *ln(σT) and Li-ion conductivity at 30 °C (303.14 K) calculated using the data (1000 E_A/k_B and $ln\sigma_0$) obtained by the linear plot of ln(σT) and 1000/T of literature data (see Table S1 and Table S2) for the $LiNH_2$, Li_2NH, $Li_2(NH_2)(BH_4)$ and $Li_4(NH_2)_3(BH_4)$. $ln(\sigma T)_{FIT}$ has been calculated using the slope and intercept obtained by the linear fit. $ln(\sigma T)_{MAX}$ and $ln(\sigma T)_{MIN}$ were calculated considering the maximum and the minimum values, of the slope and intercept, of confidence interval obtained by the linear fit. The bold (red) data were excluded in the second calculation of the average ln(σT) data. 1st and 2nd refers to the temperature-dependent EIS cycle data. CI is the confidence interval half width, calculated averaging the maximum and the $ln(\sigma T)_{MAX}$ and the $ln(\sigma T)_{MIN}$.*

References

(1) Soulie, J.; Renaudin, G.; Černý, R.; Yvon, K. Lithium Boro-Hydride $LiBH_4$ I. Crystal Structure. *J. Alloys Compd.* 2002, **346**, 200–205.

(2) Noritake, T.; Nozaki, H.; Aoki, M.; Towata, S.; Kitahara, G.; Nakamori, Y.; Orimo, S. Crystal Structure and Charge Density Analysis of Li_2NH by Synchrotron X-Ray Diffraction. *J. Alloys Compd.* 2005, **393**, 264–268.

(3) Yang, J. B.; Zhou, X. D.; Cai, Q.; James, W. J.; Yelon, W. B. Crystal and Electronic Structures of $LiNH_2$. *Appl. Phys. Lett.* 2006, **88**, 041914.

(4) Noritake, T.; Aoki, M.; Towata, S.; Ninomiya, A.; Nakamori, Y.; Orimo, S. Crystal Structure Analysis of Novel Complex Hydrides Formed by the Combination of $LiBH_4$ and $LiNH_2$. *Appl. Phys. A* 2006, **83**, 277–279.

(5) Wolczyk, A.; Paik, B.; Sato, T.; Nervi, C.; Brighi, M.; GharibDoust, S. P.; Chierotti, M.; Matsuo, M.; Li, G.; Gobetto, R.; Jensen, T. R.; Černý, R.; Orimo, S.; Baricco, M. $Li_5(BH_4)_3NH$: Lithium-Rich Mixed Anion Complex Hydride. *J. Phys. Chem. C* 2017, **121**, 11069–11075.

(6) Matsuo, M.; Nakamori, Y.; Orimo, S.; Maekawa, H.; Takamura, H. Lithium Superionic Conduction in Lithium Borohydride Accompanied by Structural Transition. *Appl. Phys. Lett.* 2007, **91**, 224103.

(7) Matsuo, M.; Takamura, H.; Maekawa, H.; Li, H.-W.; Orimo, S. Stabilization of Lithium Superionic Conduction Phase and Enhancement of Conductivity of $LiBH_4$ by LiCl Addition. *Appl. Phys. Lett.* 2009, **94**, 084103.

(8) Sveinbjörnsson, D.; Blanchard, D.; Myrdal, J. S. G.; Younesi, R.; Viskinde, R.; Riktor, M. D.; Norby, P.; Vegge, T. Ionic Conductivity and the Formation of Cubic CaH_2 in the $LiBH_4$–$Ca(BH_4)_2$ Composite. *J. Solid State Chem.* 2014, **211**, 81–89.

(9) Miyazaki, R.; Karahashi, T.; Kumatani, N.; Noda, Y.; Ando, M.; Takamura, H.; Matsuo, M.; Orimo, S.; Maekawa, H. Room Temperature Lithium Fast-Ion Conduction and Phase Relationship of LiI Stabilized $LiBH_4$. *Solid State Ionics* 2011, **192**, 143–147.

(10) Matsuo, M.; Remhof, A.; Martelli, P.; Caputo, R.; Ernst, M.; Miura, Y.; Sato, T.; Oguchi, H.; Maekawa, H.; Takamura, H.; et al. Complex Hydrides with $(BH_4)^-$ and $(NH_2)^-$ Anions as New Lithium Fast-Ion Conductors. *J. Am. Chem. Soc.* 2009, **131**, 16389–16391.

(11) Gulino, V.; Brighi, M.; Dematteis, E. M.; Murgia, F.; Nervi, C.; Černý, R.; Baricco, M. Phase Stability and Fast Ion Conductivity in the Hexagonal $LiBH_4$–LiBr–LiCl Solid Solution. *Chem. Mater.* 2019, **31**, 5133–5144.

(12) Gulino, V.; Barberis, L.; Ngene, P.; Baricco, M.; de Jongh, P. E. Enhancing Li-Ion Conductivity in $LiBH_4$-Based Solid Electrolytes by Adding Various Nanosized Oxides. *ACS*

Appl. Energy Mater. 2020, **3**, 4941–4948.

(13) Blanchard, D.; Nale, A.; Sveinbjörnsson, D.; Eggenhuisen, T. M.; Verkuijlen, M. H. W.; Suwarno; Vegge, T.; Kentgens, A. P. M.; de Jongh, P. E. Nanoconfined $LiBH_4$ as a Fast Lithium Ion Conductor. *Adv. Funct. Mater.* 2015, **25**, 184–192.

(14) Choi, Y. S.; Lee, Y.-S.; Oh, K. H.; Cho, Y. W. Interface-Enhanced Li Ion Conduction in a $LiBH_4$–SiO_2 Solid Electrolyte. *Phys. Chem. Chem. Phys.* 2016, **18**, 22540–22547.

(15) Zhou, Y.; Matsuo, M.; Miura, Y.; Takamura, H.; Maekawa, H.; Remhof, A.; Borgschulte, A.; Zuttel, A.; Otomo, T.; Orimo, S. Enhanced Electrical Conductivities of Complex Hydrides $Li_2(BH_4)(NH_2)$ and $Li_4(BH_4)(NH_2)_3$ by Melting. *Mater. Trans.* 2011, **52**, 654–657.

(16) Li, W.; Wu, G.; Xiong, Z.; Feng, Y. P.; Chen, P. Li^+ Ionic Conductivities and Diffusion Mechanisms in Li-Based Imides and Lithium Amide. *Phys. Chem. Chem. Phys.* 2012, **14**, 1596–1606.

(17) Boukamp, B. A.; Huggins, R. A. Ionic Conductivity in Lithium Imide. *Phys. Lett. A* 1979, **72**, 464–466.

(18) Yan, Y.; Kühnel, R.-S.; Remhof, A.; Duchêne, L.; Reyes, E. C.; Rentsch, D.; Łodziana, Z.; Battaglia, C. A Lithium Amide-Borohydride Solid-State Electrolyte with Lithium-Ion Conductivities Comparable to Liquid Electrolytes. *Adv. Energy Mater.* 2017, **7**, 1700294.